Published for SISSA by Springer

Received: *April 26, 2021*
Accepted: *November 27, 2021*
Published: *December 16, 2021*

Search for a heavy resonance decaying to a top quark and a W boson at $\sqrt{s} = 13$ TeV in the fully hadronic final state

The CMS collaboration

E-mail: cms-publication-committee-chair@cern.ch

Abstract: A search for a heavy resonance decaying to a top quark and a W boson in the fully hadronic final state is presented. The analysis is performed using data from proton-proton collisions at a center-of-mass energy of 13 TeV, corresponding to an integrated luminosity of 137 fb^{-1} recorded by the CMS experiment at the LHC. The search is focused on heavy resonances, where the decay products of each top quark or W boson are expected to be reconstructed as a single, large-radius jet with a distinct substructure. The production of an excited bottom quark, b^*, is used as a benchmark when setting limits on the cross section for a heavy resonance decaying to a top quark and a W boson. The hypotheses of b^* quarks with left-handed, right-handed, and vector-like chiralities are excluded at 95% confidence level for masses below 2.6, 2.8, and 3.1 TeV, respectively. These are the most stringent limits on the b^* quark mass to date, extending the previous best limits by almost a factor of two.

Keywords: Beyond Standard Model, Hadron-Hadron scattering (experiments), Heavy quark production

ArXiv ePrint: 2104.12853

https://doi.org/10.1007/JHEP12(2021)106

Contents

1 Introduction

The standard model (SM) has been extensively verified by experiment, nonetheless there exists evidence that the SM is only an effective theory. Many possibilities for physics beyond the SM have been proposed, including the possibility that quarks are composite. Such quarks would have an internal structure that, excited, could produce a state with higher mass [1, 2]. Such a phenomenon is predicted by Randall-Sundrum models [3, 4] and models with a heavy gluon partner [5–7].

In this paper, we search for a heavy resonance decaying to a top quark t and a W boson in the fully hadronic final state, using proton-proton (pp) collision data at a center-of-mass energy of 13 TeV. The search uses data corresponding to an integrated luminosity of 137 fb^{-1} recorded by the CMS experiment [8] at the CERN LHC during 2016–2018.

As a benchmark resonance, we consider an excited bottom quark, referred to as a b^* quark [2]. The strong interaction is the dominant production mechanism and can produce a single b^* quark at the LHC via the collision of a bottom quark and a gluon, $\text{bg} \to \text{b}^*$. The interaction is described by the Lagrangian

$$\mathcal{L}_1 = \frac{g_\text{s}}{2\Lambda} G_{\mu\nu} \overline{\text{b}} \sigma^{\mu\nu} \left(\kappa_\text{L}^\text{b} P_\text{L} + \kappa_\text{R}^\text{b} P_\text{R} \right) \text{b}^* + \text{h.c.}, \tag{1.1}$$

JHEP12(2021)106

where g_s is the strong coupling, $G_{\mu\nu}$ is the gauge field tensor of the gluon, $\overline{\mathrm{b}}$ is the bottom quark field, $\sigma^{\mu\nu}$ is the Pauli spin matrix, b^* is the excited bottom quark field, and Λ is the scale of compositeness [1], which is chosen to be the mass of the b^* quark. The chiral projection operators are represented as P_L and P_R, and $\kappa_\mathrm{L}^\mathrm{b}$ and $\kappa_\mathrm{R}^\mathrm{b}$ are the relative coupling strengths [9].

The $\mathrm{b}^* \to \mathrm{tW}$ decay is the dominant decay channel, with a branching fraction of approximately 40% for a b^* quark with $m_{\mathrm{b}^*} > 1.2\,\mathrm{TeV}$ [9]. The decay takes place through the weak interaction and is described by the Lagrangian

$$\mathcal{L}_2 = \frac{g_2}{\sqrt{2}} \mathrm{W}_\mu^+ \overline{\mathrm{t}} \gamma^\mu (g_\mathrm{L} P_\mathrm{L} + g_\mathrm{R} P_\mathrm{R}) \mathrm{b}^* + \mathrm{h.c.}, \tag{1.2}$$

where g_2 is the $\mathrm{SU}(2)_L$ weak coupling and g_L and g_R are the relative couplings of the W boson to the left- and right-handed b^* quark, respectively [9]. The full interaction chain is then $\mathrm{bg} \to \mathrm{b}^* \to \mathrm{tW}$. The b^* quark width is expected to be less than 10% of the b^* quark mass, which leads to a distinct resonant structure in the mass spectrum.

Three hypotheses for the left- and right-handed b^* quark couplings are considered:

$$\text{left-handed (LH):} \quad \kappa_\mathrm{L}^\mathrm{b} = g_\mathrm{L} = 1 \text{ and } \kappa_\mathrm{R}^\mathrm{b} = g_\mathrm{R} = 0, \tag{1.3}$$

$$\text{right-handed (RH):} \quad \kappa_\mathrm{L}^\mathrm{b} = g_\mathrm{L} = 0 \text{ and } \kappa_\mathrm{R}^\mathrm{b} = g_\mathrm{R} = 1, \text{ and} \tag{1.4}$$

$$\text{vector-like (LH+RH):} \quad \kappa_\mathrm{L}^\mathrm{b} = g_\mathrm{L} = 1 \text{ and } \kappa_\mathrm{R}^\mathrm{b} = g_\mathrm{R} = 1. \tag{1.5}$$

Searches for the b^* quark in the tW decay mode have been performed at the LHC by the ATLAS Collaboration at $\sqrt{s} = 7\,\mathrm{TeV}$ [10] and by the CMS Collaboration at 8 TeV [11]. Additionally, searches for a b^* quark decaying to a bottom quark and a gluon were conducted by the CMS Collaboration at 8 TeV [12] and by the ATLAS Collaboration at 13 TeV [13]. The CMS tW decay mode search included a combination of fully hadronic, lepton+jets, and dilepton final states, and excluded b^* quark masses at 95% confidence level (CL) below 1.4, 1.4, and 1.5 TeV, for the left-handed, right-handed, and vector-like hypotheses, respectively.

Given the range of these exclusions, the present analysis considers a b^* quark with a mass greater than 1.2 TeV. For these mass values, the top quark and the W boson are commonly produced with a high Lorentz boost. Because of this, the hadronic decay products of the top quark and the W boson can each merge, resulting in two massive, large-radius jets, referred to as a "top jet" and a "W jet", respectively. These jets have a distinct substructure that is used to discriminate them from the background [14, 15]. The b^* quark mass is reconstructed as the invariant mass of the top jet and W jet system, m_tW. This variable, along with the reconstructed top jet mass, m_t, is used to search for the b^* quark resonance.

The background is dominated by jets produced through the strong interaction, referred to as quantum chromodynamics (QCD) multijet production, and is estimated using multijet-enriched control regions based on inverting the top jet selection criteria. The SM W+jets and Z+jets production backgrounds are also accounted for with this technique. The $\mathrm{t\overline{t}}$ background is estimated with simulation templates fit to data simultaneously in the signal region and a dedicated control region enhanced in $\mathrm{t\overline{t}}$ production that constrains the simulation templates.

JHEP12(2021)106

A binned maximum likelihood fit to data is performed in the two-dimensional m_{tW} versus m_{t} distribution, in a process where the signal and background models are fit simultaneously. From this fit, b^* quark mass limits are derived for the three b^* chirality hypotheses expressed in eqs. (1.3), (1.4), and (1.5).

In addition, we interpret the results under the hypothesis of a singly produced B singlet vector-like quark [16, 17] decaying into tW. For B quark masses above 1.2 TeV, the decay products would be heavily boosted with a similar signature to the b^* quark decay described above. In the model considered, the $V^{\mathrm{L}}_{\mathrm{tB}}$ mixing parameter defined in ref. [16] is set to unity, which results in a relative signal width of less than 5% in the B mass range of interest, with a branching fraction to tW of approximately 50%. In contrast to the b^* model, the B quark would be produced via an electroweak interaction in association with a top or bottom quark. We consider both scenarios, but typically the associated top or bottom quark has a much lower transverse momentum than the B quark decay products, thus the effect of either on the analysis is small.

2 The CMS detector

The central feature of the CMS apparatus is a superconducting solenoid of 6 m internal diameter, providing a magnetic field of 3.8 T. Within the solenoid volume are a silicon pixel and strip tracker, a lead tungstate crystal electromagnetic calorimeter (ECAL), and a brass and scintillator hadron calorimeter (HCAL), each composed of a barrel and two endcap sections. Forward calorimeters extend the pseudorapidity coverage provided by the barrel and endcap detectors. Muons are detected in gas-ionization chambers embedded in the steel flux-return yoke outside the solenoid. A more detailed description of the CMS detector, together with a definition of the coordinate system used and the relevant kinematic variables, can be found in ref. [8].

Events of interest are selected using a two-tiered trigger system [18]. The first level, composed of custom hardware processors, uses information from the calorimeters and muon detectors to select events at a rate of around 100 kHz within a fixed latency of about 4 μs. The second level, known as the high-level trigger, consists of a farm of processors running a version of the full event reconstruction software optimized for fast processing, and reduces the event rate to around 1 kHz before data storage.

The analysis reflects the fact that the pixel detector was changed in the winter of 2016/2017. The newer detector increased the number of barrel layers from three to four and decreased the distance of the innermost layer from the beamline in order to improve the vertex reconstruction.

3 Data and simulated samples

CMS data taking operates on annual cycles, and thus data collection and simulation performance can change from year to year. Therefore, we categorize both the data and simulation by year and apply dedicated scale factors before combining the distributions from all three years to derive the final result.

JHEP12(2021)106

We analyze events from the 2016 data set recorded by a trigger that requires the scalar sum of transverse momenta, p_{T}, of all jets in the event, H_{T}, to be at least 800 or 900 GeV, or the presence of a jet with $p_{\mathrm{T}} > 450$ GeV. For 2017 and 2018 data, we analyze events recorded by a trigger that requires a minimum H_{T} of 1050 GeV or the presence of a jet with $p_{\mathrm{T}} > 500$ GeV. Additionally, 2018 data events are recorded by a trigger that requires a jet with $p_{\mathrm{T}} > 400$ GeV with a mass of at least 30 GeV, where the jet trimming algorithm [19] has been used to reconstruct the jet mass at the trigger level. This trigger did not exist for the 2016 or 2017 data collection, but the addition of events recorded by this trigger provides a higher overall selection efficiency at lower H_{T} for 2018. The choice of higher H_{T} and jet p_{T} thresholds used for 2017 and 2018 are due to an increase in the instantaneous luminosity of the LHC between 2016 and 2017. The combination of these triggers is nearly fully efficient for $m_{\mathrm{tW}} > 1200$ GeV.

The efficiency of the trigger selection is measured in data as the ratio of the number of events recorded by the combined triggers to the number of events recorded by a trigger that requires a muon candidate with $p_{\mathrm{T}} > 50$ GeV. A muon trigger is used for this measurement because it is largely uncorrelated with the triggers used for data taking.

The trigger efficiencies are parameterized as a function of dijet invariant mass (m_{jj}) and both the numerator and denominator of the ratio include events that pass the preselection described in section 5. The uncertainty assigned to the efficiency measurement is one half of the trigger inefficiency.

Figure 1 shows the trigger efficiency derived from 2016, 2017, and 2018 data separately. Simulated samples are corrected using the efficiency measurement from the corresponding data-taking year.

A trigger inefficiency referred to as "prefiring" occurred during the 2016 and 2017 data taking. Over that time period, a gradual shift in the timing of triggering systems based on the ECAL in the endcap caused certain events to not be recorded. Event corrections were calculated from data and applied to the 2016 and 2017 simulations to model this inefficiency. The uncertainties in these corrections are taken as systematic uncertainties.

The SM $\mathrm{t\bar{t}}$ and single top quark Monte Carlo (MC) simulated samples are used as templates for background estimation in the maximum likelihood fit to data. A scale factor is applied to the generated top quark p_{T} spectrum to correct for the differences between data and $\mathrm{t\bar{t}}$ simulation. It is based on a dedicated measurement [20, 21], in which the ratio of the distribution of the top quark p_{T} measured in data to the distribution as measured in POWHEG+PYTHIA is derived. This scale factor may be described by the expression

$$w_{\mathrm{t}}(p_{\mathrm{T}}) = \mathrm{e}^{c_1 0.0615 - c_2 (0.0005/\,\mathrm{GeV}) p_{\mathrm{T}}}, \tag{3.1}$$

where c_1 and c_2 are taken to be 1, as obtained in refs. [20, 21]. The p_{T}-dependent event weight is given by $\sqrt{w_{\mathrm{t}}(p_{\mathrm{T}}) w_{\bar{\mathrm{t}}}(p_{\mathrm{T}})}$, where $w_{\mathrm{t}}(p_{\mathrm{T}})$ and $w_{\bar{\mathrm{t}}}(p_{\mathrm{T}})$ are evaluated using the top quark and antiquark p_{T}, respectively. We use the same form for the scale factor but treat c_1 and c_2 as fit parameters initialized to 1 and constrained in the fit to a Gaussian with a width of 0.5.

To simulate the SM $\mathrm{t\bar{t}}$ and single top quark production, we use the POWHEG v2 [22–26] matrix element event generator. For QCD multijet simulation, we use

JHEP12(2021)106

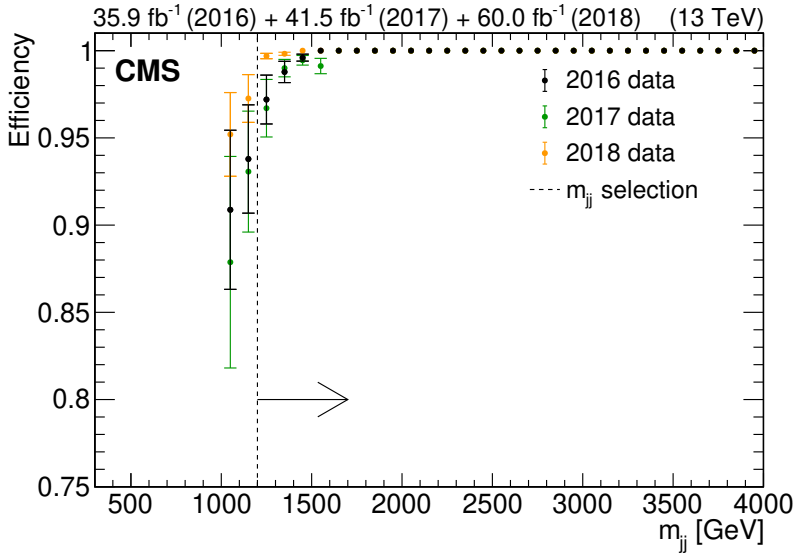

Figure 1. The efficiency of the full trigger selection as a function of m_{jj}, shown separately for 2016, 2017, and 2018 data. The minimum m_{jj} considered in the analysis is 1200 GeV and is marked with a dashed line and an arrow. The efficiency below m_{jj} of 1000 GeV is not measured. The points for 2017 and 2018 data are not visible in the plateau because they are overlapped by the points for 2016 data.

MadGraph5_*a*mc@nlo version 5 [27] with subversion 2.2.2 for 2016 and 2.4.2 for 2017 and 2018. The QCD multijet simulated samples are used to derive a scale factor to the multijet background estimation procedure and for cross checks of self consistency of the background estimate. The b^* signal samples are simulated using MadGraph5_*a*mc@nlo version 5 over a mass range of 1.4 to 4.0 TeV in steps of 200 GeV. Subversion 2.2.2 is used for 2016 b^* signal samples with b^* quark masses from 1.4 to 3.0 TeV and 2016 B+t and B+b signal samples. Subversion 2.4.2 is used for 2017 and 2018 b^* signal samples with b^* quark masses from 1.4 to 3.0 TeV. Subversion 2.6.5 is used for all b^* signal samples with b^* quark masses above 3.0 TeV. For the B signal simulations, we use samples based on the 2016 conditions and scale the final distributions to the integrated luminosity of the full data set, after correcting for differences in annual selection efficiencies that are measured with the b^* signal samples. We simulate B quark masses from 1.4 to 1.8 TeV in steps of 100 GeV.

Hadronization and parton showering are simulated using the pythia 8 software package [28]. The NNPDF3.0 [29] parton distribution functions (PDFs) are used with the CUETP8M1 [30] underlying event tune for the 2016 simulations and the NNPDF3.1 [31] PDFs are used with the CP5 [32] underlying event tune for the 2017 and 2018 simulations. The CMS detector simulation is performed with Geant4 [33]. Pythia version 8.212 is used for all the 2016 simulations with the exception of 2016 b^* signal samples with b^* quark masses from 1.4 to 3.0 TeV, which use version 8.226, and 2016 B signal samples, which use version 8.205. Pythia version 8.230 is used for all the 2017 and 2018 simulations.

To simulate the effect of additional pp collision data within the same or adjacent bunch crossings (pileup), additional inelastic events are superimposed using pythia. Simulated

JHEP12(2021)106

samples are then reweighted to correct the pileup simulation, using the total inelastic cross section of 69 mb [34, 35] to estimate the distribution of the number of primary vertices in data.

4 Event reconstruction

The candidate vertex with the largest value of summed physics-object p_{T}^2 is taken to be the primary pp interaction vertex. The physics objects are the jets, clustered using the anti-k_{T} jet finding algorithm [36, 37] with a distance parameter of $R = 0.4$ and with the tracks assigned to candidate vertices as inputs, and the associated missing transverse momentum, taken as the negative vector sum of the transverse momentum of those jets.

A particle-flow algorithm [38] aims to reconstruct and identify each individual particle in an event, with an optimized combination of information from the various elements of the CMS detector. The energy of muons is obtained from the curvature of the corresponding track. The energy of charged hadrons is determined from a combination of their momentum measured in the tracking detector and the matching ECAL and HCAL energy deposits, corrected for the response function of the calorimeters to hadronic showers. Finally, the energy of neutral hadrons is obtained from the corresponding corrected ECAL and HCAL energies. Jets are clustered with the anti-k_{T} jet finding algorithm, using all particle-flow objects as input. Jet momentum is determined as the vectorial sum of all particle momenta in the jet. Jets with a distance parameter of $R = 0.8$ are used to reconstruct the top jet and W jet candidates in an event.

The pileup per particle identification (PUPPI) algorithm [39] is used to mitigate the effect of pileup at the reconstructed particle level, making use of local shape information, event pileup properties, and tracking information. A local shape variable is defined, which distinguishes between collinear and soft diffuse distributions of other particles surrounding the particle under consideration. The former is attributed to particles originating from the hard scatter and the latter to particles originating from pileup interactions. Charged particles originating from pileup vertices are discarded. For each neutral particle, a local shape variable is computed using the surrounding charged particles compatible with the primary vertex within the tracking detector acceptance ($|\eta| < 2.5$), and using both charged and neutral particles in the region outside of the tracking detector coverage. The momenta of the neutral particles are then rescaled according to the probability that they originate from the primary interaction vertex as deduced from the local shape variable, superseding the need for jet-based pileup corrections [40].

Jet energy corrections are derived from simulation studies so that the average measured response of jets becomes identical to that of the jets from the reconstructed particle level. In situ measurements of the momentum balance in dijet, photon+jet, Z+jet, and multijet events are used to determine any residual differences between the jet energy scale in data and in simulation, and appropriate corrections are made [41]. Additional selection criteria are applied to each jet to remove jets potentially dominated by instrumental effects or reconstruction failures [42].

JHEP12(2021)106

4.1 Top quark identification

The soft-drop algorithm [43], a generalization of the modified mass drop algorithm [44, 45], with angular exponent $\beta = 0$ and soft threshold $z = 0.1$, is applied to all jets in the event to reconstruct the jet mass and to identify subjets, and includes a grooming step to remove soft radiation, including pileup. We only consider top jets with a minimum soft-drop mass of 65 GeV.

The N-subjettiness algorithm [46] defines τ_N variables, which describe the consistency between the jet energy deposits and the number of assumed subjets, N. When compared to jets originating from a gluon or a light quark, a top jet is more consistent with three hard decay products, and the ratio of τ_3 and τ_2 allows top jets to be distinguished from QCD multijet background [47]. A lower ratio indicates the jet is more consistent with a three-pronged structure than a two-pronged structure.

The b^* signal region selection requires $\tau_3/\tau_2 < 0.65$. The N-subjettiness ratios are correlated with the jet mass, so a relatively loose selection for the signal region is used to avoid biasing the mass distribution of multijet processes.

We also require the top jet to contain a subjet from the soft-drop algorithm to be identified as a bottom quark by the DeepCSV algorithm [48]. The combination of the τ_3/τ_2 and DeepCSV selections has a QCD jet misidentification rate of approximately 1% and a top tag signal efficiency of approximately 45% [42, 49]. This selection has been chosen because it leads to an optimal sensitivity of the cross section limits.

A jet that passes both the τ_3/τ_2 and DeepCSV b tagging selection is considered "top tagged". A p_{T}-dependent correction is applied to correct for differences in the top tagging efficiency between data and simulation [49]. Separate corrections are used based upon the merging of the top quark decay products in simulation. Taking the line defined by the top quark's trajectory as the central axis, three scenarios are considered. In the first, the three decay products are within $R < 0.8$ of the central axis and the jet is considered "merged". In the second, two out of three decay products are within $R < 0.8$ of the central axis and the jet is "semi-merged". Finally, with any other configuration of the three decay products the jet is "not merged". The merged component is the dominant contribution for the b^* signal process among these three scenarios.

4.2 W boson identification

Similar to top tagging, the W boson identification algorithm requires a selection based on τ_N and soft-drop mass. The W jet is required to have a soft-drop mass between 65 and 105 GeV to be consistent with the W boson mass [50]. The ratio of N-subjettiness τ_2 and τ_1 variables is used to select the characteristic two-prong structure of a hadronic W boson decay since the W jet is more consistent with having two subjets than one. The b^* signal region selection requires $\tau_2/\tau_1 < 0.4$ for 2016 data and simulation, and $\tau_2/\tau_1 < 0.45$ for 2017 and 2018 data and simulation. The combined selection on the mass and τ_2/τ_1 has a QCD jet misidentification rate of approximately 10% and a W tag signal efficiency of approximately 80%, which are consistent across the three years [42, 49]. This selection was chosen because it leads to an optimal sensitivity of the cross section limits.

JHEP12(2021)106

A jet that passes the τ_2/τ_1 and soft-drop mass selections is considered "W tagged". Differences in the W tagging efficiency between data and simulation are corrected using simulation-to-data weights [49]. Additionally, differences in the soft-drop mass scale and resolution between data and simulation are accounted for by scaling and smearing the soft-drop mass in simulation [42].

5 Event selection

To select signal-like events, two jets are required with $p_T > 400\,\text{GeV}$ and $|\eta| < 2.4$. Only the two jets with the highest p_T are considered in the following. The jets are required to satisfy that the difference in rapidity, $|\Delta y|$, be less than 1.6 and that $|\Delta\phi|$ be greater than $\pi/2$. The $|\Delta\phi|$ requirement selects back-to-back dijet events while the $|\Delta y|$ requirement suppresses multijet events with high m_{tW}, which arise from the scattering of valence quarks. These requirements comprise the "preselection", with an event then being selected as signal if one of the two jets is W tagged and the other is top tagged.

Because the background estimate relies on data in a control region defined by inverting the top tag selection, we first require that one of the two jets can be identified as a W jet. In the case that both jets can be W tagged, the jet with lower p_T is taken as the W boson candidate in the event. If neither jet can be W tagged, the event is not selected. The jet that is taken as the W boson candidate is referred to as the initially tagged or first jet and the other jet is called the remaining or second jet. If the event is selected, it is categorized in either the signal region or the multijet control region depending on whether the second jet passes the top tagging requirement. The final selection efficiency for simulated events is calculated as the number of events that pass the signal selection divided by the number of events generated. Over the range of generated b^* quark masses, signals with left-handed couplings are selected with an efficiency of 9–10%. Signals with right-handed couplings have slightly higher efficiencies, ranging from 10–11%, because of their harder jet p_T spectra.

We additionally define a dedicated $t\bar{t}$ measurement region. For this, events are required to pass the preselection but the W tag is changed to a top tag selection for the initial jet tag. This jet tag also requires a top jet mass value between 105 and 220 GeV to be consistent with the top quark mass [50]. The second top tag will be used to distribute events between the $t\bar{t}$ measurement region selection and the dedicated multijet control region for the $t\bar{t}$ measurement region. Additionally, for the initial jet tag, the subjet bottom quark requirement remains the same but a tighter selection of $\tau_3/\tau_2 < 0.54$ is required. The tighter selection on the initial jet tag increases the relative $t\bar{t}$ contribution. The τ_3/τ_2 selection on the second jet tag remains the same as for the b^* signal region selection to avoid distorting the mass distribution because of the correlation described in section 4.1. If both jets fulfill the selection of the initial top tag, the jet with the lower p_T is takes as the initially top tagged jet in the event. The $t\bar{t}$ background measurement region is described in more detail in section 6.2. The four tagging selection regions are summarized in table 1.

Comparisons of the N-subjettiness ratio, soft-drop mass, and DeepCSV algorithm score in simulation between signal and background events are shown in figure 2. The QCD contribution to the multijet background is shown, but the W+jets and Z+jets contributions

JHEP12(2021)106

	W tag	Top tag
Top tag	Signal region (SR)	$\mathrm{t\bar{t}}$ measurement region ($\mathrm{t\bar{t}}$MR)
Inverted top tag	Multijet control region (for SR)	Multijet control region (for $\mathrm{t\bar{t}}$MR)

Table 1. A summary of the four selection regions considered in the likelihood fit to data. The columns indicate the possible jet tag for the jet considered in the preselection while the rows indicate the possible classification of the second jet when using the top tagging algorithm.

are omitted since simulations of these processes are not used in this analysis (as discussed in section 6.1).

6 Statistical model and background estimation

The background for this analysis is comprised of multijet, $\mathrm{t\bar{t}}$, and tW-channel single top production. The multijet component is estimated from data while the $\mathrm{t\bar{t}}$ and single top components are obtained by fitting simulation templates to data.

The m_{t} range considered is larger than the signal mass window of 105 to 220 GeV defined in section 5. As shown in figure 2, an m_{t} selection is not efficient at discriminating signal from $\mathrm{t\bar{t}}$ background. However, by using m_{t} as one of the two measurement dimensions, one can constrain the multijet background in the m_{t} sidebands while distinguishing the multijet background from the top quark backgrounds in the m_{t} signal region. Thus, the m_{t} range comprises both the signal peak region and the lower and upper sidebands of the peak. The signal region considers the range of 65 to 285 GeV while the $\mathrm{t\bar{t}}$ measurement region exists between 105 and 285 GeV, where the lower mass bound of 105 GeV is used to ensure the orthogonality with the W jet mass window of the signal region.

For each bin in the two-dimensional $(m_{\mathrm{t}}, m_{\mathrm{tW}})$ distribution, we compare the number of expected events from both the background-only and signal-plus-background hypotheses with the number of observed events in data.

The expected number of events from b^* quark production is calculated as $N_{\text{expected}} = \sigma_{\mathrm{b}^*}\mathcal{B}(\mathrm{b}^* \to \mathrm{tW} \to \text{hadrons})\varepsilon L$, where σ_{b^*} is the b^* quark cross section, $\mathcal{B}(\mathrm{b}^* \to \mathrm{tW} \to \text{hadrons})$ is the branching fraction of $\mathrm{b}^* \to \mathrm{tW}$ in the fully hadronic decay mode, ε is the product of the acceptance and the efficiency, and L is the integrated luminosity of the data set.

A likelihood fit to data is used to test the signal hypothesis, where the total background model is constructed as a sum of the individual background contributions using a Poisson model for each bin of the $(m_{\mathrm{t}}, m_{\mathrm{tW}})$ distribution.

The number of expected events with failing, n_{F}, and passing, n_{P}, top tags in a given bin is given by

$$n_{\mathrm{F}}(i,\vec{\theta}) = n_{\mathrm{F}}^{\mathrm{QCD}}(i) + n_{\mathrm{F}}^{\mathrm{t\bar{t}}}(i,\vec{\theta}) + n_{\mathrm{F}}^{\text{single top}}(i,\vec{\theta}) + n_{\mathrm{F}}^{\text{signal}}(i,\vec{\theta}) \tag{6.1}$$

$$n_{\mathrm{P}}(i,\vec{\theta}) = n_{\mathrm{P}}^{\mathrm{QCD}}(i) + n_{\mathrm{P}}^{\mathrm{t\bar{t}}}(i,\vec{\theta}) + n_{\mathrm{P}}^{\text{single top}}(i,\vec{\theta}) + n_{\mathrm{P}}^{\text{signal}}(i,\vec{\theta}), \tag{6.2}$$

where i is a bin in the $(m_{\mathrm{t}}, m_{\mathrm{tW}})$ plane, and $\vec{\theta}$ is the set of all nuisance parameters that quantify the systematic uncertainties, as described in section 7. The variable $n_{\mathrm{F}}^{\mathrm{QCD}}(i)$ is an

JHEP12(2021)106

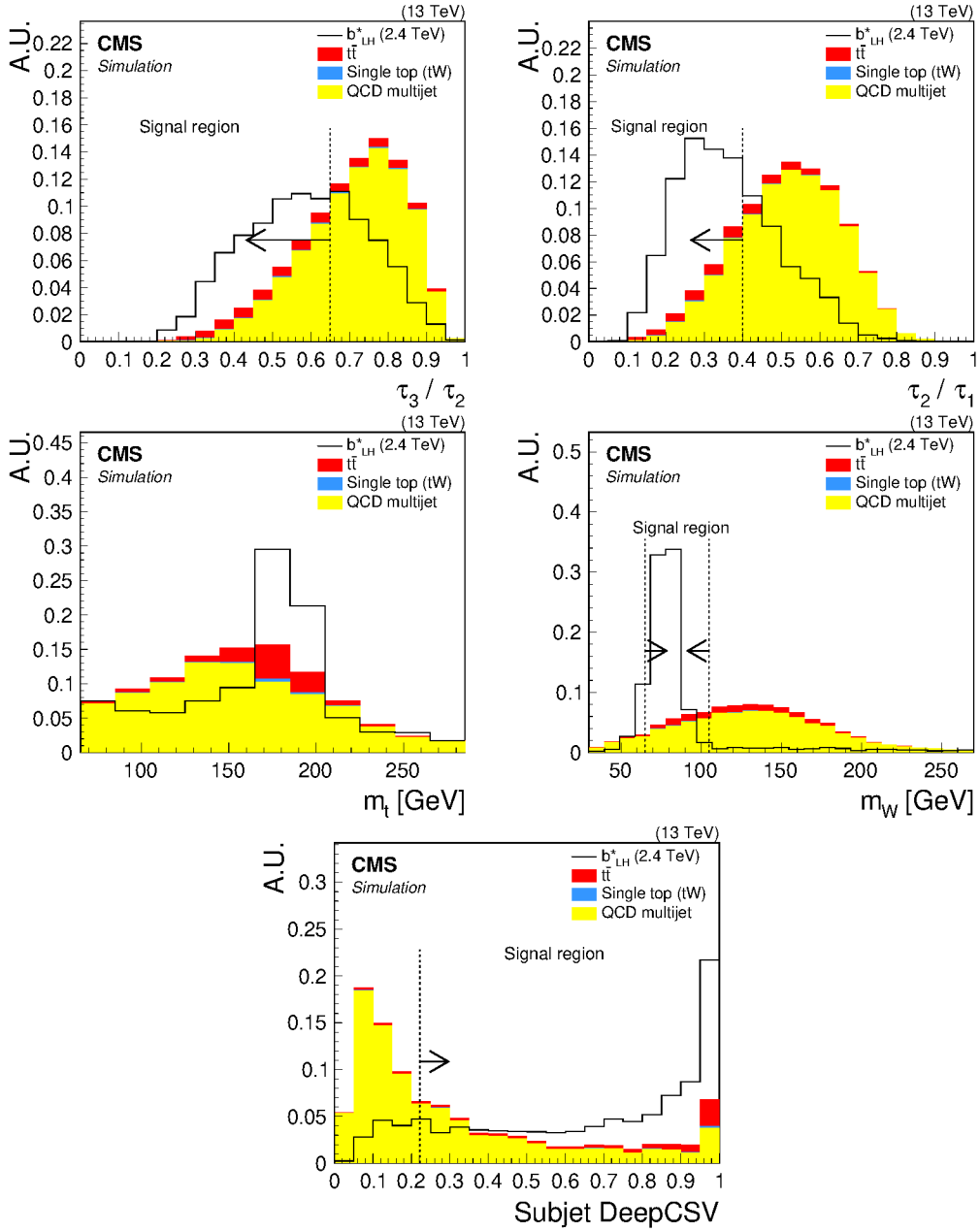

Figure 2. The distributions of the discrimination variables used for W and top tagging for simulation samples. These plots show the top jet τ_3/τ_2 (upper left), the W jet τ_2/τ_1 (upper right), the top tag soft-drop mass (middle left), the W tag soft-drop mass (middle right), and the subjet b-tagging discriminant (lower). The b^* signal sample is represented with the solid line. The area of the total background contribution and the area of the signal component are separately normalized to unity. All analysis selections of the signal region are applied with the exception of the variable being plotted. Also shown are vertical dashed lines and arrows, which indicate the optimized selection used for events in the signal region. For the b^* signal sample, the top tag soft-drop mass spectrum exhibits a resonance in the first bin near the W mass, which is comprised of W jets that have been misidentified as top jets.

JHEP12(2021)106

unconstrained positive real number. Finally, $n_{\mathrm{P}}^{\mathrm{QCD}}(i)$ is given by

$$n_{\mathrm{P}}^{\mathrm{QCD}}(i) = n_{\mathrm{F}}^{\mathrm{QCD}}(i) f(m_{\mathrm{t}}, m_{\mathrm{tW}}), \tag{6.3}$$

where $f(m_{\mathrm{t}}, m_{\mathrm{tW}})$ is a transfer function defined by the ratio of top tagging pass and fail events, and is described in section 6.1.

The negative log-likelihood is then

$$-\ln L(\vec{d};\vec{\theta}) = \sum_{i=1}^{N_{\mathrm{bins,F}}} \left[n_{\mathrm{F}}(i,\vec{\theta}) - d_{\mathrm{F}}(i) \ln n_{\mathrm{F}}(i,\vec{\theta}) \right] + \sum_{i=1}^{N_{\mathrm{bins,P}}} \left[n_{\mathrm{P}}(i,\vec{\theta}) - d_{\mathrm{P}}(i) \ln n_{\mathrm{P}}(i,\vec{\theta}) \right], \tag{6.4}$$

where $N_{\mathrm{bins,F}}$ and $N_{\mathrm{bins,P}}$ are the total number of bins and $d_{\mathrm{F}}(i)$ and $d_{\mathrm{P}}(i)$ are the number of observed events in a given bin, for the fail and pass distributions, respectively. Thus, there is one likelihood which combines four separate categories — signal region "pass" and "fail" and $\mathrm{t\bar{t}}$ measurement region "pass" and "fail".

6.1 Multijet background estimate

After applying the kinematic selection along with the W jet identification, we define the ratio of the multijet background distributions that pass and fail the top tagging requirement in data and QCD multijet MC simulation as $R_{\mathrm{P/F}}^{\mathrm{data}}(m_{\mathrm{t}}, m_{\mathrm{tW}})$ and $R_{\mathrm{P/F}}^{\mathrm{MC}}(m_{\mathrm{t}}, m_{\mathrm{tW}})$, respectively. Because of the combinatorial nature of multijet processes, $R_{\mathrm{P/F}}^{\mathrm{data}}(m_{\mathrm{t}}, m_{\mathrm{tW}})$ and $R_{\mathrm{P/F}}^{\mathrm{MC}}(m_{\mathrm{t}}, m_{\mathrm{tW}})$ are both smooth as a function of m_{t} and m_{tW}. The data-to-simulation ratio of these ratios is therefore also smooth and can be used to correct for differences in simulation and data by parameterizing it with an analytic function, $R_{\mathrm{ratio}}(m_{\mathrm{t}}, m_{\mathrm{tW}})$.

While $R_{\mathrm{P/F}}^{\mathrm{data}}(m_{\mathrm{t}}, m_{\mathrm{tW}})$ could also be described by analytic functions, isolated features of the shape can be factored out by using simulation. By factoring out $R_{\mathrm{P/F}}^{\mathrm{MC}}(m_{\mathrm{t}}, m_{\mathrm{tW}})$, the fit of the analytic function to data is only responsible for describing the residual differences between data and simulation that can be parameterized with fewer parameters than the shape of $R_{\mathrm{P/F}}^{\mathrm{data}}(m_{\mathrm{t}}, m_{\mathrm{tW}})$.

The number of events in a given bin of the passing category can then be estimated from the equation

$$n_{\mathrm{P}}^{\mathrm{QCD}}(i) = n_{\mathrm{F}}^{\mathrm{QCD}}(i) R_{\mathrm{P/F}}^{\mathrm{MC}}(m_{\mathrm{t}}, m_{\mathrm{tW}}) R_{\mathrm{ratio}}(m_{\mathrm{t}}, m_{\mathrm{tW}}), \tag{6.5}$$

where $f(m_{\mathrm{t}}, m_{\mathrm{tW}})$ has been replaced by $R_{\mathrm{P/F}}^{\mathrm{MC}}(m_{\mathrm{t}}, m_{\mathrm{tW}}) R_{\mathrm{ratio}}(m_{\mathrm{t}}, m_{\mathrm{tW}})$ and $R_{\mathrm{ratio}}(m_{\mathrm{t}}, m_{\mathrm{tW}})$ is a surface parameterized by the product of two one-dimensional polynomials in the $(m_{\mathrm{t}}, m_{\mathrm{tW}})$ plane with coefficients determined from the fit to data. A second-order polynomial was chosen for the m_{t} axis and a first-order polynomial was chosen for the m_{tW} axis. These choices were based on a Fisher test [51] where polynomial terms were added until the p-value obtained in the test was less than 0.95. The parameters of the two-dimensional polynomials are uncorrelated between years. The form of $R_{\mathrm{ratio}}(m_{\mathrm{t}}, m_{\mathrm{tW}})$ is then

$$(p_0 + p_1 m_{\mathrm{t}} + p_2 m_{\mathrm{t}}^2)(1 + p_3 m_{\mathrm{tW}}). \tag{6.6}$$

JHEP12(2021)106

To reduce the effect of statistical fluctuations when calculating $R^{\mathrm{MC}}_{\mathrm{P/F}}(m_{\mathrm{t}}, m_{\mathrm{tW}})$ in the QCD multijet simulation, the pass and fail distributions are smoothed by using an adaptive kernel density estimate [52] (KDE) prior to calculating the ratio. Additionally, the residual contributions from the W+jets and Z+jets backgrounds are accounted for in this analysis, as they are absorbed by the unconstrained $R_{\mathrm{ratio}}(m_{\mathrm{t}}, m_{\mathrm{tW}})$ function.

6.2 Top quark measurement region

By performing the maximum likelihood fit to data in the signal region simultaneously with the $\mathrm{t\bar{t}}$ background enriched measurement region, we further constrain the $\mathrm{t\bar{t}}$ contribution to the total background estimate. In particular, this region is used to make measurements of the c_1 and c_2 fit parameters of eq. (3.1).

The $\mathrm{t\bar{t}}$ measurement region is evaluated in the $(m_{\mathrm{t}}, m_{\mathrm{tt}})$ plane, where m_{t} is the mass of the second jet when using the top tagging algorithm and m_{tt} is the invariant mass of the $\mathrm{t\bar{t}}$ pair. Only the multijet and $\mathrm{t\bar{t}}$ SM processes are considered in this selection since the single top quark contribution is negligible.

The strategy to estimate the multijet background in the $\mathrm{t\bar{t}}$ measurement region is similar to the signal region. The $R^{\mathrm{t\bar{t}MR}}_{\mathrm{ratio}}(m_{\mathrm{t}}, m_{\mathrm{tt}})$ in this region is parameterized with the same polynomial form as in the signal region, but the parameters are uncorrelated with those of the signal region. Additionally, the $R^{\mathrm{MC}}_{\mathrm{P/F}}(m_{\mathrm{t}}, m_{\mathrm{tt}})$ is derived using QCD multijet simulation events that pass the same selection as the $\mathrm{t\bar{t}}$ measurement region. Events from W+jets and Z+jets backgrounds are suppressed by the initial top tag requirement, and any that remain are accounted for by the multijet background model as they are in the signal region.

The negative log-likelihood calculated from the $\mathrm{t\bar{t}}$ measurement region is constructed similarly to eq. (6.4). The total negative log-likelihood is obtained from the sum of the negative log-likelihoods of the signal region and the $\mathrm{t\bar{t}}$ measurement region. Because the fit to data can constrain the $\mathrm{t\bar{t}}$ background in both selections, the values of the free parameters that determine the shape and normalization of the $\mathrm{t\bar{t}}$ simulation are constrained by the simultaneous fit to the $\mathrm{t\bar{t}}$- and signal-enriched selections.

7 Systematic uncertainties

This analysis takes into account several systematic uncertainties that can affect both the shape and normalization of the simulation.

Normalization uncertainties include those in the production cross section and in the measured integrated luminosity of the data. The uncertainties in the $\mathrm{t\bar{t}}$ and single top tW-channel production are taken as 20 and 30%, respectively, to account for the uncertainties in the cross section and in the factorization and renormalization scales of each process. Specifically, these values were chosen based on the largest variations in yield of the simulated samples from varying the factorization and renormalization scales. The uncertainty in the measured integrated luminosity is 1.8% [53–55] for the complete Run 2 (2016–2018).

Several uncertainties exist that affect both the shape and normalization of the $(m_{\mathrm{t}}, m_{\mathrm{tW}})$ distributions. The uncertainties in the jet energy scale and resolution are estimated through variations in p_{T} and η of the PUPPI jets [41]. The uncertainty in the pileup reweighting

JHEP12(2021)106

correction is evaluated by varying the total inelastic cross section by ±4.6% [34]. The uncertainty in the trigger correction is taken into account as a variation of one half of the trigger inefficiency. The uncertainty in the PDFs is derived by either evaluating the root-mean-square of the set of NNPDF MC replicas or by evaluating the contributions of eigenvectors provided in a Hessian set [56], depending on whether the PDF set represents variations as MC replicas or Hessian eigenvectors. The uncertainty due to differences in the data and simulation efficiency for the top jet tagging algorithm is evaluated by using the variations of the top tagging scale factor [49]. The scale factors and uncertainties vary depending on the merging scenarios defined in section 4.1. The W tagging uncertainty is evaluated from variations in the W tagging scale factor and includes an additional uncertainty when extrapolating to jets outside of the p_{T} region used to extract the scale factor. Additionally, the uncertainty in the W tagging soft-drop mass selection is evaluated from variations in the jet mass scale and resolution [49]. No variations in the jet mass scale and resolution are considered for the candidate top jet since the effect is negligible with respect to the current results.

Unique to the $\mathrm{t\bar{t}}$ simulation is the uncertainty in the top quark p_{T} reweighting procedure described in section 3, which is extrapolated to high p_{T}. The uncertainty is represented as uncorrelated variations of ±50% in each of the c_1 and c_2 parameters from eq. (3.1).

Each uncertainty affecting both the shape and normalization is Gaussian constrained where the ±1 standard deviation of each distribution is mapped to the ±1 standard deviation of the corresponding unit Gaussian constraint.

The uncertainty in the multijet background estimation is taken from the maximum likelihood fit to data. The parameters of each two-dimensional polynomial are uncorrelated and fitted freely with no *a-priori* constraints. An additional uncertainty in the "bandwidth" parameter of the KDE algorithm is accounted for by varying the parameter up and down by 1, where the nominal value is 4. This parameter acts as a scale to determine the width of the adaptive kernels.

All systematic uncertainties are considered in the simultaneous fit to data such that all correlations are preserved. The uncertainties are always correlated across tW and $\mathrm{t\bar{t}}$ selections within a given year of data and simulation. The cross section, PDF, and top quark p_{T} reweighting c_1 and c_2 uncertainties are individually correlated across the data-taking years. Table 2 summarizes the sources of uncertainty and indicates where correlations between samples exist.

Additionally, table 2 includes a calculation of the "impact" of a parameter on the measurement of the final signal strength for a 2.4 TeV b^* quark signal. This value is calculated by comparing the measured signal strength in the full fit against the measured signal strength in a fit where the given nuisance parameter has been changed either "up" or "down" one standard deviation from its post-fit value in the full fit.

As can be seen in table 2, the multijet estimate from data is the dominant source of background uncertainty in the measurement of the signal strength. In particular, variations of one post-fit standard deviation of the linear term in the m_{tW} axis of the signal region can change the measurement of the signal strength by approximately 19%.

JHEP12(2021)106

Source	Uncertainty	Samples	Impact Up	Impact Down
$t\bar{t}$ cross section	±20%	$t\bar{t}$	−4.6	+4.4%
Single top cross section	±30%	Single top	+1.2	−1.4%
Integrated luminosity	±1.8%	$t\bar{t}$, single top, signal	+1.6	−1.1%
Pileup	Shape (σ_{mb})	$t\bar{t}$, single top, signal	+0.3	−0.2%
Trigger prefiring	Shape (p_T, η)	$t\bar{t}$, single top, signal	+0.0	+0.1%
Jet energy scale	Shape (p_T)	$t\bar{t}$, single top, signal	+0.3	−0.6%
Jet energy resolution	Shape (p_T, η)	$t\bar{t}$, single top, signal	−0.4	−0.5%
Jet mass scale	Shape (m_W)	$t\bar{t}$, single top, signal	−0.1	−0.0%
Jet mass resolution	Shape (m_W)	$t\bar{t}$, single top, signal	+0.0	+0.9%
W tagging	Shape (p_T)	Single top, signal	+0.9	−0.9%
W tagging: p_T extrapolation	Shape (p_T)	Single top, signal	+4.9	−4.9%
Top tagging, merged	Shape (p_T)	$t\bar{t}$, single top, signal	+0.2	−0.2%
Top tagging, semimerged	Shape (p_T)	$t\bar{t}$, single top, signal	+1.1	−0.9%
Top tagging, not merged	Shape (p_T)	$t\bar{t}$, single top, signal	−0.1	+0.1%
Trigger	Shape (H_T)	$t\bar{t}$, single top, signal	+0.3	−0.4%
Top quark p_T correction c_1	Shape (p_T)	$t\bar{t}$	−0.3	+0.3%
Top quark p_T correction c_2	Shape (p_T)	$t\bar{t}$	−3.9	+3.5%
PDF	Shape (m_t, m_{tW})	Signal	+0.1	−0.1%
KDE bandwidth	Shape (m_t, m_{tW})	Multijet (from simulation)	−1.2	+0.2%
$R^{SR}_{ratio}(m_t, m_{tW})p_0$	Shape (m_t, m_{tW})	Multijet (from data)	−4.4	+0.0%
$R^{SR}_{ratio}(m_t, m_{tW})p_1$	Shape (m_t, m_{tW})	Multijet (from data)	−2.0	+2.2%
$R^{SR}_{ratio}(m_t, m_{tW})p_2$	Shape (m_t, m_{tW})	Multijet (from data)	+0.9	−0.8%
$R^{SR}_{ratio}(m_t, m_{tW})p_3$	Shape (m_t, m_{tW})	Multijet (from data)	+18.6	−18.8%
$R^{t\bar{t}MR}_{ratio}(m_t, m_{tt})p_0$	Shape (m_t, m_{tt})	Multijet (from data)	−0.4	+0.6%
$R^{t\bar{t}MR}_{ratio}(m_t, m_{tt})p_1$	Shape (m_t, m_{tt})	Multijet (from data)	−0.4	+0.6%
$R^{t\bar{t}MR}_{ratio}(m_t, m_{tt})p_2$	Shape (m_t, m_{tt})	Multijet (from data)	+0.5	−0.6%
$R^{t\bar{t}MR}_{ratio}(m_t, m_{tt})p_3$	Shape (m_t, m_{tt})	Multijet (from data)	−0.6	+0.6%

Table 2. Sources of uncertainty that are taken into account in the statistical analysis of the data. The sources affecting the normalization are given with their percentage uncertainties, while the sources affecting the shape are listed as "Shape" together with the dependent parameter. The rightmost column indicates the impact of the parameter on the 2.4 TeV b^* signal strength when the parameter is changed "up" and "down" by one standard deviation from its post-fit value. For parameters where the uncertainties are uncorrelated between data-taking years, the average impact is calculated. An impact of +0.0 (−0.0) denotes an impact that is less (greater) than 0.1 (−0.1) but greater (less) than 0.

JHEP12(2021)106

8 Results

The $(m_{\mathrm{t}}, m_{\mathrm{tW}})$ and $(m_{\mathrm{t}}, m_{\mathrm{tt}})$ distributions are used in a simultaneous binned maximum likelihood fit to data. The signal strength is a free parameter in the model and the systematic uncertainties are accounted for as nuisance parameters as described in section 6. Normalization uncertainties are modeled with log-normal priors, and uncertainties affecting simulation shapes are modeled using a template morphing approach with Gaussian priors.

While the fit is performed in two dimensions, evaluating the agreement of the background model with the data is more convenient when examining projections onto one dimension. The background estimate and measured two-dimensional distributions from the simultaneous fit of the signal region, $\mathrm{t\bar{t}}$ measurement region, and multijet-enriched control regions are shown in figures 3 and 4, respectively, as one-dimensional projections where either the m_{tt} or m_{t} distribution has been separated into three regions. The lower panels show the pull, defined as the difference between the number of events observed in the data and the predicted background, divided by the systematic uncertainty in the background and the statistical uncertainty in the data, added in quadrature. All plots shown are for the signal-plus-background hypothesis post-fit, where the 2.4 TeV $\mathrm{b}^*_{\mathrm{LH}}$ quark sample is normalized to the post-fit signal cross section.

In figure 3, the left column shows distributions of m_{t} obtained for the selection of the $\mathrm{t\bar{t}}$ measurement region, but with a jet failing the top tagging requirement. The right column shows the same distributions, but for jets passing the top tagging requirement. The rows give the distributions for separate intervals of m_{tt}. The background estimation is observed to model the data well in both regions, validating the estimation of the multijet background and the modeling of the $\mathrm{t\bar{t}}$ simulation. The contribution from a possible signal is negligible in this region and therefore not visible.

In figure 4, distributions of m_{tW}, obtained for events passing the signal region selection are shown, where the distributions in the left and right columns have been obtained for jets failing and passing the top tagging requirement, respectively. Plots in the row are for separate intervals of m_{t}. The total background estimate agrees with the data within the uncertainties. The largest excess in data relative to the total background is observed for a left-handed b^* quark with a mass of 2.4 TeV, which results in a local significance of 2.3 standard deviations.

Additionally, the post-fit top quark p_{T} reweighting measurements are consistent with the pre-fit values, and are measured to be $c_1 = 1.01 \pm 0.25$ and $c_2 = 1.16 \pm 0.16$. The agreement of the background-only model is evaluated using the saturated test statistic [57, 58] and has a p-value of 0.3. Additionally, the post-fit nuisance parameter values are consistent with the pre-fit values and the nuisance parameter values from the background-only model fit are consistent with those from the signal-plus-background model fit.

Asymptotic frequentist statistics are used to derive exclusion limits on $\sigma_{\mathrm{b}^*}\mathcal{B}(\mathrm{b}^* \to \mathrm{tW} \to \text{hadrons})$ at 95% CL [59]. These limits are derived separately for the $\mathrm{b}^*_{\mathrm{RH}}$, $\mathrm{b}^*_{\mathrm{LH}}$, and $\mathrm{b}^*_{\mathrm{LH+RH}}$ quark signal hypotheses. The ± 1 and ± 2 standard deviations in the expected limit are derived from pseudo-experiments under the background-only hypothesis in which the nuisance parameters are randomly varied within the post-fit constraints of the maximum likelihood fit to data.

JHEP12(2021)106

The limits are shown in figure 5. The theoretical b^* cross sections included in the figure as a function of b^* quark mass are calculated using MadGraph5_*a*mc@nlo. Masses below 2.6, 2.8, and 3.1 TeV (2.9, 3.0, and 3.3 TeV) are observed (expected) to be excluded at 95% CL for the left-handed, right-handed, and vector-like hypotheses, respectively. These limits nearly doubles the mass exclusions of the previous result [11].

The sensitivity of this analysis can also be compared to the sensitivity of the CMS dijet search [60]. The branching fraction for $b^* \to bg$ approaches 20% asymptotically for high masses [9]. From the dijet search, the expected upper limit on the product of the cross section and branching fraction for a resonance decaying to a quark and a gluon is approximately 0.09 pb at 2 TeV so the cross section upper limit on b^* quark production is approximately 0.45 pb. Using the left-handed couplings result in figure 5, this analysis achieves an expected upper limit of approximately 0.015 pb at 2 TeV. With the $b^* \to tW$ branching fraction of 0.4, the cross section upper limit on b^*_{LH} quark production at 2 TeV is approximately 0.0375 pb. Thus, at 2 TeV, this search is about an order of magnitude more sensitive to the excited b^* quark than the dijet search.

The results of this search can also be used to test models of a single B quark produced via the electroweak interaction in association with a bottom or top quark, and decaying into a top quark and a W boson. Because the cross section for this process is much smaller than for a b^* quark produced through the strong force, and because of the selection $m_{tW} > 1.2$ TeV, we consider the mass range 1.4 to 1.8 TeV in this interpretation. The exclusion limits on $\sigma_B \mathcal{B}(B \to tW \to \text{hadrons})$ at 95% CL are shown in figure 6. Over the mass range of 1.4–1.8 TeV, the observed upper limit ranges 0.027 to 0.009 pb when produced in association with a bottom quark and from 0.036 to 0.012 pb when produced in association with a top quark. Because of the small theoretical cross section for the model considered, no mass limit is set. When compared to the b^* quark in this mass range, the expected cross section upper limits for a B quark produced with an associated bottom quark are uniformly more sensitive by approximately 22%. The equivalent comparison for a B quark produced with an associated top quark shows the sensitivity is worse by no more than 7%.

These results based on 137 fb^{-1} of data can be compared directly to those of ref. [61], which analyzed the lepton+jets channel in 35.9 fb^{-1} of data recorded with the CMS experiment at $\sqrt{s} = 13$ TeV. At a B quark mass of 1.4 TeV, this analysis is less sensitive than the results from ref. [61] by about 20% when considering B quark production with an associated top quark. However, this analysis has about 20% higher sensitivity than the previous analysis when the production is in association with a bottom quark. As the B quark mass increases, the sensitivity of this analysis increases faster than the analysis described in ref. [61]. Thus, the sensitivity of this analysis at 1.8 TeV is about 27% higher for the associated top quark hypothesis and about a factor of two higher for the associated bottom quark hypothesis. This comparison is also applicable to the results for a left-handed B hypothesis in ref. [62], which analyzed the lepton+jets channel in 36.1 fb^{-1} of data recorded with the ATLAS experiment at $\sqrt{s} = 13$ TeV and which has comparable results to those in ref. [61].

JHEP12(2021)106

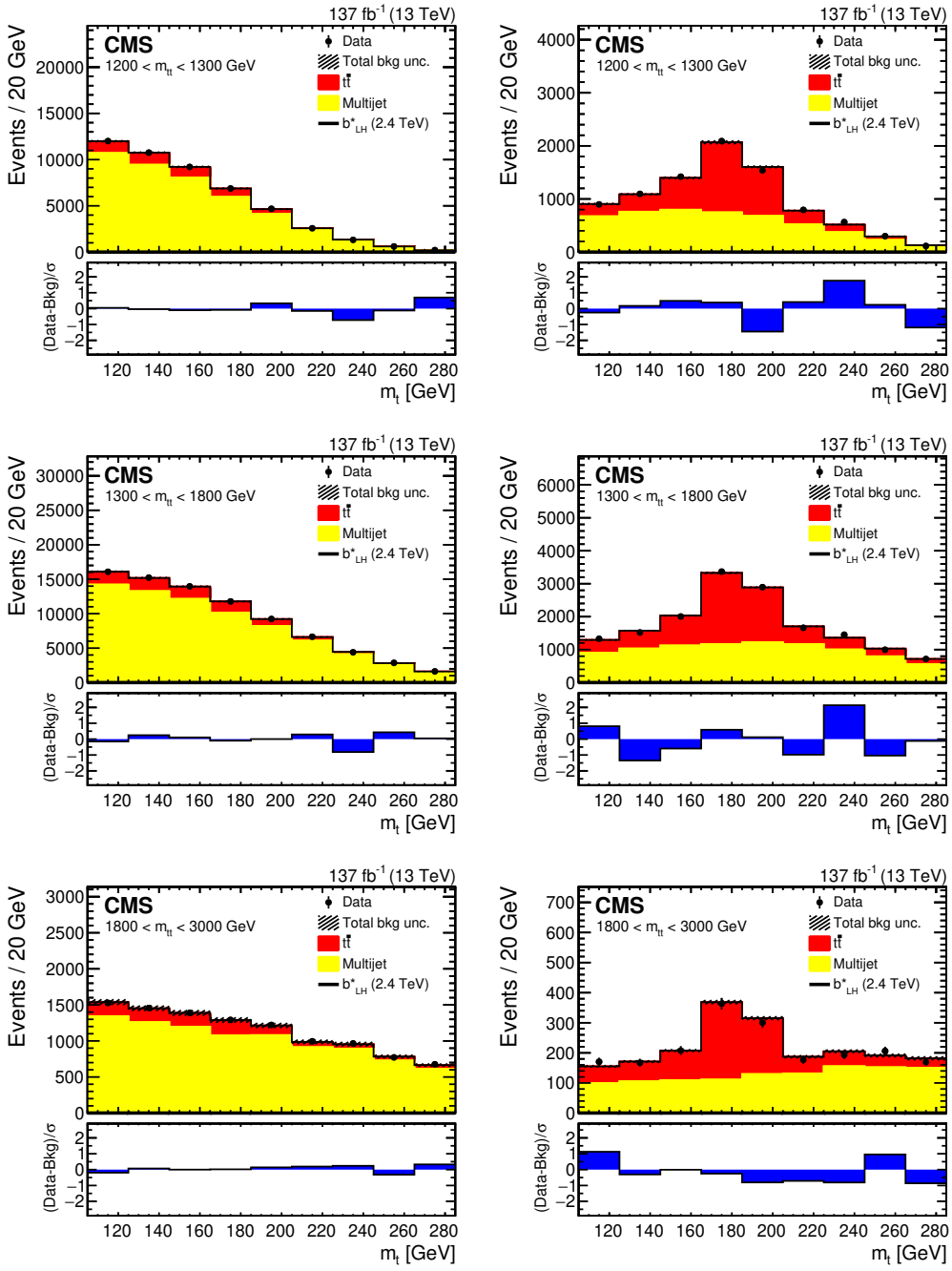

Figure 3. Distributions of m_{t} in the $\mathrm{t\bar{t}}$ measurement region for three intervals of m_{tt}: 1200–1300 GeV (upper), 1300–1800 GeV (middle), 1800–3000 GeV (lower). The data are shown by points with error bars and the individual background contributions by filled histograms. The signal is not visible because the contamination in this region is negligible. The barely visible shaded region is the uncertainty in the total background estimate. The left and right columns show distributions for events with the second jet failing and passing the top tagging requirement, respectively. The lower panels of each figure show the pull, as a function of m_{t}, defined as the difference between the number of events observed in the data and the predicted background, divided by their combined uncertainty.

JHEP12(2021)106

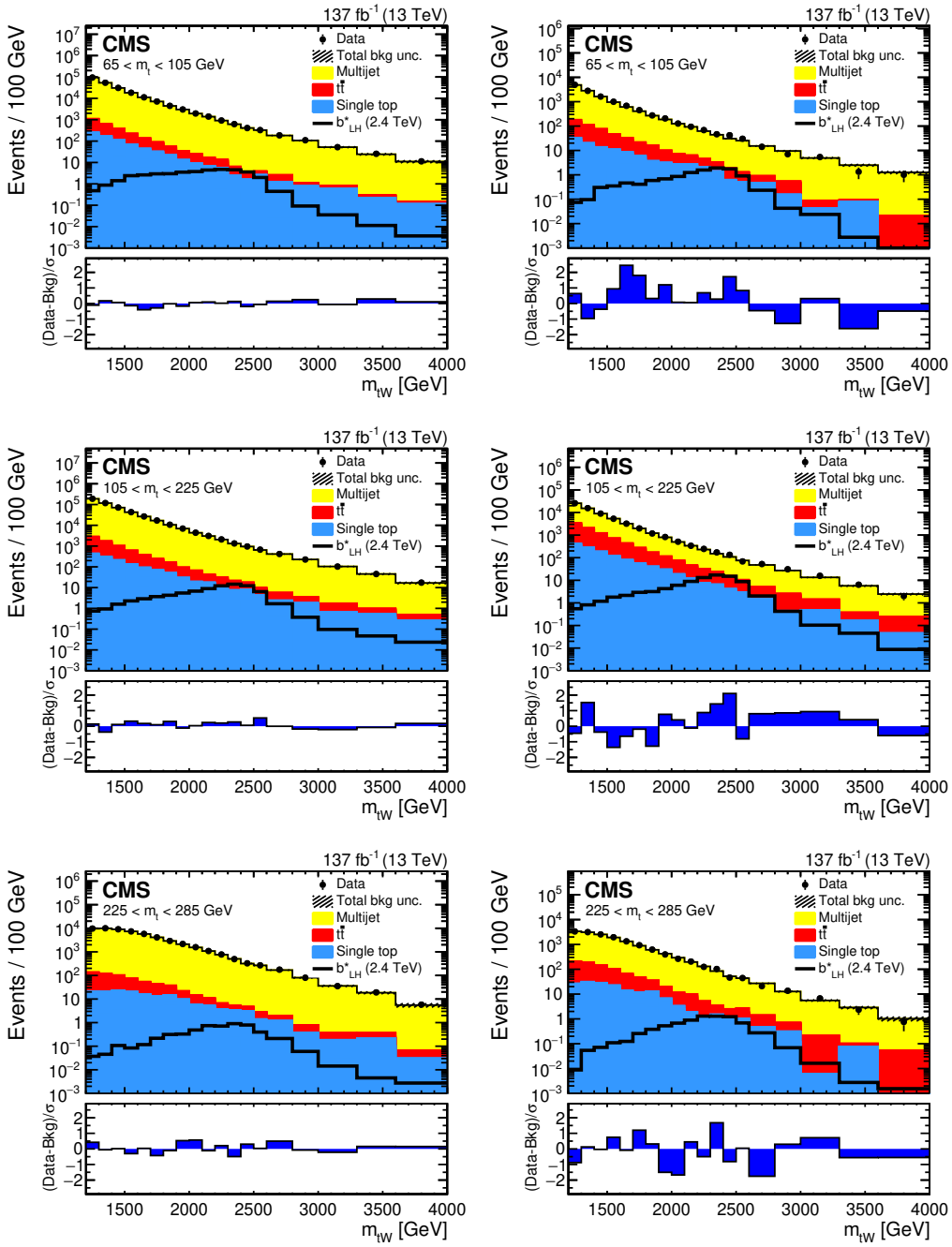

Figure 4. Distributions of m_{tW} in the b^* signal region for three intervals of m_{t}: 65–105 GeV (upper), 105–225 GeV (middle), and 225–285 GeV (lower). The data are shown by points with error bars, the individual background contributions by filled histograms, and a 2.4 TeV $\mathrm{b}^*_{\mathrm{LH}}$ signal is shown as a solid line. The barely visible shaded region is the uncertainty in the total background estimate. The left and right columns show distributions for events with a jet failing and passing the top tagging requirement, respectively. The lower panels of each figure show the pull, as a function of m_{tW}, defined as the difference between the number of events observed in the data and the predicted background, divided by their combined uncertainty.

JHEP12(2021)106

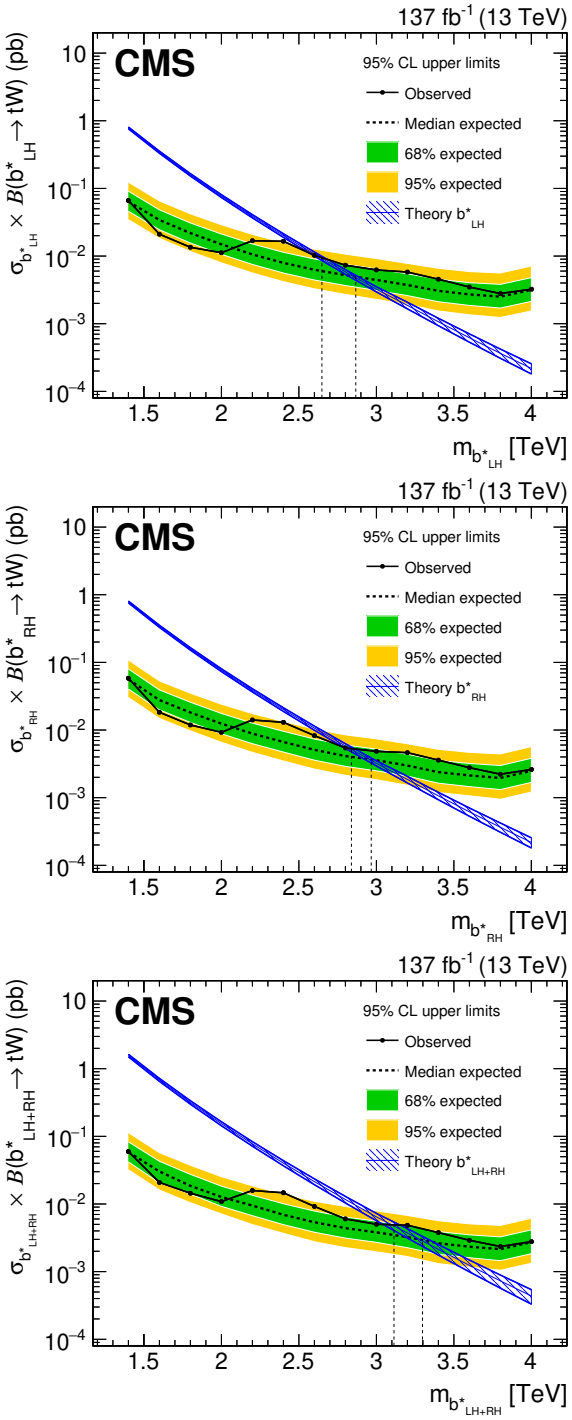

Figure 5. Upper limits on the product of the cross section and branching fraction at 95% CL for a b^*_{LH} (upper), b^*_{RH} (middle), and b^*_{LH+RH} (lower) quark as a function of the b^* quark mass. The expected (dashed) and observed (dot-solid) limits, as well as the b^* quark theoretical cross sections (shaded-solid), are shown. The vertical dashed lines indicate the intersection of the theoretical cross sections with the expected and observed limits. The inner and outer shaded areas around the expected limits show the 68% and 95% CL intervals, respectively.

JHEP12(2021)106

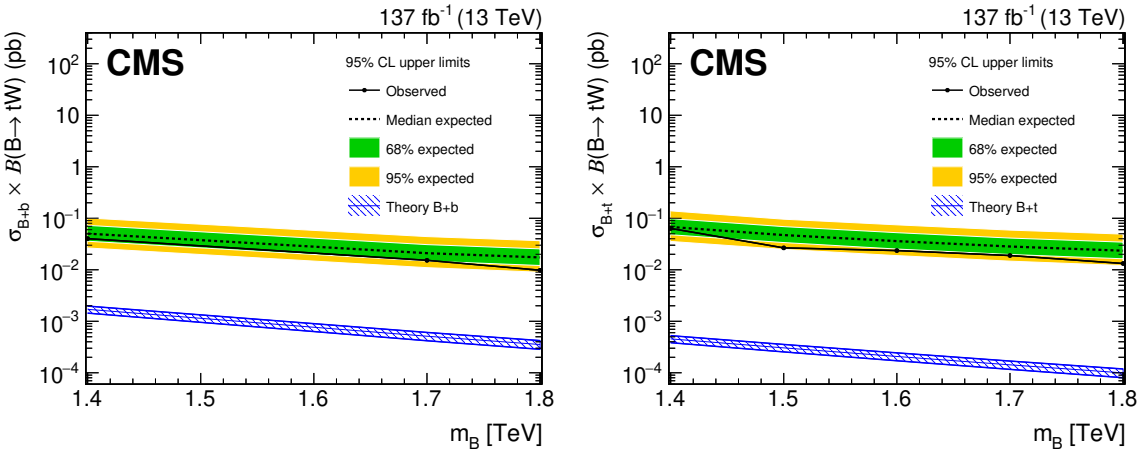

Figure 6. Upper limits on the product of the cross section and branching fraction at 95% CL for a B produced in association with a bottom quark (left) and top quark (right) as a function of the B quark mass. The expected (dashed) and observed (dot-solid) limits, as well as the B quark theoretical cross sections (shaded-solid), are shown. The inner and outer shaded areas around the expected limits show the 68% and 95% CL intervals, respectively.

9 Summary

A search for a heavy resonance decaying to a top quark and a W boson in the fully hadronic final state has been presented. The analysis uses proton-proton collision data at a center-of-mass energy of 13 TeV corresponding to an integrated luminosity of 137 fb^{-1}, collected by the CMS experiment at the LHC during 2016–2018.

This analysis considers the explicit case where the heavy resonance is an excited bottom quark, b*. The search evaluates b* quark masses greater than 1.2 TeV, which result in highly Lorentz-boosted top quarks and W bosons that are reconstructed as single jets. Using jet substructure algorithms designed to distinguish heavy resonance decays from light-quark and gluon jets, the top quark and W boson decays are identified as a top quark jet and a W boson jet, respectively.

The background processes in the analysis are a result of multijet processes from the strong interaction, $\mathrm{t\bar{t}}$ production, and single top quark (tW-channel) production. The search is performed using a two-dimensional binned likelihood fit to the data that allows all backgrounds to be fit simultaneously. The multijet component in the signal region is estimated via a two-dimensional transfer function method that uses a multijet-enriched control region. The $\mathrm{t\bar{t}}$ and single top background estimates are determined via a template fit to data. In particular, a dedicated $\mathrm{t\bar{t}}$ measurement region is used to constrain the shape and yield of the $\mathrm{t\bar{t}}$ background.

No statistically significant deviation from the standard model expectation is observed. The hypotheses of b* quarks with left-handed, right-handed, and vector-like chiralities are excluded at 95% confidence level for masses below 2.6, 2.8, and 3.1 TeV, respectively. These are the most stringent limits on the b* quark mass to date, extending the previous best mass limits by almost a factor of two.

JHEP12(2021)106

Acknowledgments

We congratulate our colleagues in the CERN accelerator departments for the excellent performance of the LHC and thank the technical and administrative staffs at CERN and at other CMS institutes for their contributions to the success of the CMS effort. In addition, we gratefully acknowledge the computing centers and personnel of the Worldwide LHC Computing Grid and other centers for delivering so effectively the computing infrastructure essential to our analyses. Finally, we acknowledge the enduring support for the construction and operation of the LHC, the CMS detector, and the supporting computing infrastructure provided by the following funding agencies: BMBWF and FWF (Austria); FNRS and FWO (Belgium); CNPq, CAPES, FAPERJ, FAPERGS, and FAPESP (Brazil); MES (Bulgaria); CERN; CAS, MoST, and NSFC (China); MINCIENCIAS (Colombia); MSES and CSF (Croatia); RIF (Cyprus); SENESCYT (Ecuador); MoER, ERC PUT and ERDF (Estonia); Academy of Finland, MEC, and HIP (Finland); CEA and CNRS/IN2P3 (France); BMBF, DFG, and HGF (Germany); GSRT (Greece); NKFIA (Hungary); DAE and DST (India); IPM (Iran); SFI (Ireland); INFN (Italy); MSIP and NRF (Republic of Korea); MES (Latvia); LAS (Lithuania); MOE and UM (Malaysia); BUAP, CINVESTAV, CONACYT, LNS, SEP, and UASLP-FAI (Mexico); MOS (Montenegro); MBIE (New Zealand); PAEC (Pakistan); MSHE and NSC (Poland); FCT (Portugal); JINR (Dubna); MON, RosAtom, RAS, RFBR, and NRC KI (Russia); MESTD (Serbia); SEIDI, CPAN, PCTI, and FEDER (Spain); MOSTR (Sri Lanka); Swiss Funding Agencies (Switzerland); MST (Taipei); ThEPCenter, IPST, STAR, and NSTDA (Thailand); TUBITAK and TAEK (Turkey); NASU (Ukraine); STFC (United Kingdom); DOE and NSF (U.S.A.).

Individuals have received support from the Marie-Curie program and the European Research Council and Horizon 2020 Grant, contract Nos. 675440, 724704, 752730, 765710 and 824093 (European Union); the Leventis Foundation; the Alfred P. Sloan Foundation; the Alexander von Humboldt Foundation; the Belgian Federal Science Policy Office; the Fonds pour la Formation à la Recherche dans l'Industrie et dans l'Agriculture (FRIA-Belgium); the Agentschap voor Innovatie door Wetenschap en Technologie (IWT-Belgium); the F.R.S.-FNRS and FWO (Belgium) under the "Excellence of Science — EOS" — be.h project n. 30820817; the Beijing Municipal Science & Technology Commission, No. Z191100007219010; the Ministry of Education, Youth and Sports (MEYS) of the Czech Republic; the Deutsche Forschungsgemeinschaft (DFG), under Germany's Excellence Strategy — EXC 2121 "Quantum Universe" — 390833306, and under project number 400140256 — GRK2497; the Lendület ("Momentum") Program and the János Bolyai Research Scholarship of the Hungarian Academy of Sciences, the New National Excellence Program ÚNKP, the NKFIA research grants 123842, 123959, 124845, 124850, 125105, 128713, 128786, and 129058 (Hungary); the Council of Science and Industrial Research, India; the Ministry of Science and Higher Education and the National Science Center, contracts Opus 2014/15/B/ST2/03998 and 2015/19/B/ST2/02861 (Poland); the National Priorities Research Program by Qatar National Research Fund; the Ministry of Science and Higher Education, project no. 0723-2020-0041 (Russia); the Programa Estatal de Fomento de la Investigación Científica y Técnica de Excelencia María de Maeztu, grant MDM-2015-0509 and the Programa Severo

JHEP12(2021)106

Ochoa del Principado de Asturias; the Thalis and Aristeia programs cofinanced by EU-ESF and the Greek NSRF; the Rachadapisek Sompot Fund for Postdoctoral Fellowship, Chulalongkorn University and the Chulalongkorn Academic into Its 2nd Century Project Advancement Project (Thailand); the Kavli Foundation; the Nvidia Corporation; the SuperMicro Corporation; the Welch Foundation, contract C-1845; and the Weston Havens Foundation (U.S.A.).

JHEP12(2021)106

References

[1] U. Baur, M. Spira and P.M. Zerwas, *Excited-quark and -lepton production at hadron colliders*, *Phys. Rev. D* **42** (1990) 815 [INSPIRE].

[2] T.M.P. Tait and C.P. Yuan, *Single top quark production as a window to physics beyond the standard model*, *Phys. Rev. D* **63** (2000) 014018 [hep-ph/0007298] [INSPIRE].

[3] C. Cheung, A.L. Fitzpatrick and L. Randall, *Sequestering CP violation and GIM-violation with warped extra dimensions*, *JHEP* **01** (2008) 069 [arXiv:0711.4421] [INSPIRE].

[4] A.L. Fitzpatrick, G. Perez and L. Randall, *Flavor anarchy in a Randall-Sundrum model with 5D minimal flavor violation and a low Kaluza-Klein scale*, *Phys. Rev. Lett.* **100** (2008) 171604 [arXiv:0710.1869] [INSPIRE].

[5] C. Bini, R. Contino and N. Vignaroli, *Heavy-light decay topologies as a new strategy to discover a heavy gluon*, *JHEP* **01** (2012) 157 [arXiv:1110.6058] [INSPIRE].

[6] N. Vignaroli, *Discovering the composite Higgs through the decay of a heavy fermion*, *JHEP* **07** (2012) 158 [arXiv:1204.0468] [INSPIRE].

[7] N. Vignaroli, $\Delta F = 1$ *constraints on composite Higgs models with left-right parity*, *Phys. Rev. D* **86** (2012) 115011 [arXiv:1204.0478] [INSPIRE].

[8] CMS collaboration, *The CMS experiment at the CERN LHC*, 2008 *JINST* **3** S08004 [INSPIRE].

[9] J. Nutter, R. Schwienhorst, D.G.E. Walker and J.-H. Yu, *Single top production as a probe of B' quarks*, *Phys. Rev. D* **86** (2012) 094006 [arXiv:1207.5179] [INSPIRE].

[10] ATLAS collaboration, *Search for single b^*-quark production with the ATLAS detector at $\sqrt{s} = 7$ TeV*, *Phys. Lett. B* **721** (2013) 171 [arXiv:1301.1583] [INSPIRE].

[11] CMS collaboration, *Search for the production of an excited bottom quark decaying to tW in proton-proton collisions at $\sqrt{s} = 8$ TeV*, *JHEP* **01** (2016) 166 [arXiv:1509.08141] [INSPIRE].

[12] CMS collaboration, *Search for resonances and quantum black holes using dijet mass spectra in proton-proton collisions at $\sqrt{s} = 8$ TeV*, *Phys. Rev. D* **91** (2015) 052009 [arXiv:1501.04198] [INSPIRE].

[13] ATLAS collaboration, *Search for new resonances in mass distributions of jet pairs using 139 fb^{-1} of pp collisions at $\sqrt{s} = 13$ TeV with the ATLAS detector*, *JHEP* **03** (2020) 145 [arXiv:1910.08447] [INSPIRE].

[14] A.J. Larkoski, I. Moult and B. Nachman, *Jet substructure at the Large Hadron Collider: A review of recent advances in theory and machine learning*, *Phys. Rept.* **841** (2020) 1 [arXiv:1709.04464] [INSPIRE].

[15] R. Kogler et al., *Jet substructure at the Large Hadron Collider*, *Rev. Mod. Phys.* **91** (2019) 045003 [arXiv:1803.06991] [INSPIRE].

[16] J.A. Aguilar-Saavedra, R. Benbrik, S. Heinemeyer and M. Pérez-Victoria, *Handbook of vectorlike quarks: Mixing and single production*, *Phys. Rev. D* **88** (2013) 094010 [arXiv:1306.0572] [INSPIRE].

[17] A. De Simone, O. Matsedonskyi, R. Rattazzi and A. Wulzer, *A first top partner hunter's guide*, *JHEP* **04** (2013) 004 [arXiv:1211.5663] [INSPIRE].

[18] CMS collaboration, *The CMS trigger system*, 2017 *JINST* **12** P01020 [arXiv:1609.02366] [INSPIRE].

[19] D. Krohn, J. Thaler and L.-T. Wang, *Jet Trimming*, *JHEP* **02** (2010) 084 [arXiv:0912.1342] [INSPIRE].

[20] CMS collaboration, *Measurements of* $\mathrm{t\bar{t}}$ *differential cross sections in proton-proton collisions at* $\sqrt{s} = 13$ *TeV using events containing two leptons*, *JHEP* **02** (2019) 149 [arXiv:1811.06625] [INSPIRE].

[21] CMS collaboration, *Measurement of differential cross sections for top quark pair production using the lepton+jets final state in proton-proton collisions at* 13 *TeV*, *Phys. Rev. D* **95** (2017) 092001 [arXiv:1610.04191] [INSPIRE].

[22] E. Re, *Single-top Wt-channel production matched with parton showers using the POWHEG method*, *Eur. Phys. J. C* **71** (2011) 1547 [arXiv:1009.2450] [INSPIRE].

[23] P. Nason, *A new method for combining NLO QCD with shower Monte Carlo algorithms*, *JHEP* **11** (2004) 040 [hep-ph/0409146] [INSPIRE].

[24] S. Frixione, P. Nason and C. Oleari, *Matching NLO QCD computations with parton shower simulations: The POWHEG method*, *JHEP* **11** (2007) 070 [arXiv:0709.2092] [INSPIRE].

[25] S. Alioli, P. Nason, C. Oleari and E. Re, *A general framework for implementing NLO calculations in shower Monte Carlo programs: The POWHEG BOX*, *JHEP* **06** (2010) 043 [arXiv:1002.2581] [INSPIRE].

[26] S. Frixione, P. Nason and G. Ridolfi, *A positive-weight next-to-leading-order Monte Carlo for heavy flavour hadroproduction*, *JHEP* **09** (2007) 126 [arXiv:0707.3088] [INSPIRE].

[27] J. Alwall et al., *The automated computation of tree-level and next-to-leading order differential cross sections and their matching to parton shower simulations*, *JHEP* **07** (2014) 079 [arXiv:1405.0301] [INSPIRE].

[28] T. Sjöstrand et al., *An introduction to PYTHIA 8.2*, *Comput. Phys. Commun.* **191** (2015) 159 [arXiv:1410.3012] [INSPIRE].

[29] NNPDF collaboration, *Parton distributions for the LHC Run II*, *JHEP* **04** (2015) 040 [arXiv:1410.8849] [INSPIRE].

[30] CMS collaboration, *Event generator tunes obtained from underlying event and multiparton scattering measurements*, *Eur. Phys. J. C* **76** (2016) 155 [arXiv:1512.00815] [INSPIRE].

[31] NNPDF collaboration, *Parton distributions from high-precision collider data*, *Eur. Phys. J. C* **77** (2017) 663 [arXiv:1706.00428] [INSPIRE].

JHEP12(2021)106

[32] CMS collaboration, *Extraction and validation of a new set of CMS PYTHIA8 tunes from underlying-event measurements*, *Eur. Phys. J. C* **80** (2020) 4 [arXiv:1903.12179] [INSPIRE].

[33] GEANT4 collaboration, GEANT4 — *a simulation toolkit*, *Nucl. Instrum. Meth. A* **506** (2003) 250 [INSPIRE].

[34] ATLAS collaboration, *Measurement of the inelastic proton-proton cross section at* $\sqrt{s} = 13$ *TeV with the ATLAS Detector at the LHC*, *Phys. Rev. Lett.* **117** (2016) 182002 [arXiv:1606.02625] [INSPIRE].

[35] CMS collaboration, *Measurement of the inelastic proton-proton cross section at* $\sqrt{s} = 13$ *TeV*, *JHEP* **07** (2018) 161 [arXiv:1802.02613] [INSPIRE].

[36] M. Cacciari, G.P. Salam and G. Soyez, *The anti-*k_t *jet clustering algorithm*, *JHEP* **04** (2008) 063 [arXiv:0802.1189] [INSPIRE].

[37] M. Cacciari, G.P. Salam and G. Soyez, *FastJet user manual*, *Eur. Phys. J. C* **72** (2012) 1896 [arXiv:1111.6097] [INSPIRE].

[38] CMS collaboration, *Particle-flow reconstruction and global event description with the CMS detector*, 2017 *JINST* **12** P10003 [arXiv:1706.04965] [INSPIRE].

[39] D. Bertolini, P. Harris, M. Low and N. Tran, *Pileup per particle identification*, *JHEP* **10** (2014) 059 [arXiv:1407.6013] [INSPIRE].

[40] CMS collaboration, *Pileup mitigation at CMS in* 13 *TeV data*, 2020 *JINST* **15** P09018 [arXiv:2003.00503] [INSPIRE].

[41] CMS collaboration, *Jet energy scale and resolution in the CMS experiment in pp collisions at* 8 *TeV*, 2017 *JINST* **12** P02014 [arXiv:1607.03663] [INSPIRE].

[42] CMS collaboration, *Jet algorithms performance in* 13 *TeV data*, CMS-PAS-JME-16-003 (2017).

[43] A.J. Larkoski, S. Marzani, G. Soyez and J. Thaler, *Soft drop*, *JHEP* **05** (2014) 146 [arXiv:1402.2657] [INSPIRE].

[44] M. Dasgupta, A. Fregoso, S. Marzani and G.P. Salam, *Towards an understanding of jet substructure*, *JHEP* **09** (2013) 029 [arXiv:1307.0007] [INSPIRE].

[45] J.M. Butterworth, A.R. Davison, M. Rubin and G.P. Salam, *Jet substructure as a new Higgs search channel at the LHC*, *Phys. Rev. Lett.* **100** (2008) 242001 [arXiv:0802.2470] [INSPIRE].

[46] J. Thaler and K. Van Tilburg, *Identifying boosted objects with* N*-subjettiness*, *JHEP* **03** (2011) 015 [arXiv:1011.2268] [INSPIRE].

[47] J. Thaler and K. Van Tilburg, *Maximizing boosted top identification by minimizing* N*-subjettiness*, *JHEP* **02** (2012) 093 [arXiv:1108.2701] [INSPIRE].

[48] CMS collaboration, *Identification of heavy-flavour jets with the CMS detector in pp collisions at* 13 *TeV*, 2018 *JINST* **13** P05011 [arXiv:1712.07158] [INSPIRE].

[49] CMS collaboration, *Identification of heavy, energetic, hadronically decaying particles using machine-learning techniques*, 2020 *JINST* **15** P06005 [arXiv:2004.08262] [INSPIRE].

[50] PARTICLE DATA GROUP collaboration, *Review of particle physics*, *PTEP* **2020** (2020) 083C01 [INSPIRE].

[51] R.A. Fisher, *On the interpretation of* χ^2 *from contingency tables and the calculation of p*, *J. Roy. Stat. Soc.* **85** (1922) 87.

JHEP12(2021)106

[52] K.S. Cranmer, *Kernel estimation in high-energy physics*, *Comput. Phys. Commun.* **136** (2001) 198 [hep-ex/0011057] [INSPIRE].

[53] CMS collaboration, *CMS luminosity measurements for the 2016 data taking period*, CMS-PAS-LUM-17-001 (2017).

[54] CMS collaboration, *CMS luminosity measurement for the 2017 data-taking period at* $\sqrt{s} = 13$ *TeV*, CMS-PAS-LUM-17-004 (2018).

[55] CMS collaboration, *CMS luminosity measurement for the 2018 data-taking period at* $\sqrt{s} = 13$ *TeV*, CMS-PAS-LUM-18-002 (2019).

[56] J. Butterworth et al., *PDF4LHC recommendations for LHC Run II*, *J. Phys. G* **43** (2016) 023001 [arXiv:1510.03865] [INSPIRE].

[57] S. Baker and R.D. Cousins, *Clarification of the use of chi square and likelihood functions in fits to histograms*, *Nucl. Instrum. Meth.* **221** (1984) 437 [INSPIRE].

[58] J.K. Lindsey, *Parametric statistical inference*, Oxford University Press, New York (1966).

[59] G. Cowan, K. Cranmer, E. Gross and O. Vitells, *Asymptotic formulae for likelihood-based tests of new physics*, *Eur. Phys. J. C* **71** (2011) 1554 [*Erratum ibid.* **73** (2013) 2501] [arXiv:1007.1727] [INSPIRE].

[60] CMS collaboration, *Search for high mass dijet resonances with a new background prediction method in proton-proton collisions at* $\sqrt{s} = 13$ *TeV*, *JHEP* **05** (2020) 033 [arXiv:1911.03947] [INSPIRE].

[61] CMS collaboration, *Search for single production of vector-like quarks decaying to a top quark and a W boson in proton-proton collisions at* $\sqrt{s} = 13$ *TeV*, *Eur. Phys. J. C* **79** (2019) 90 [arXiv:1809.08597] [INSPIRE].

[62] ATLAS collaboration, *Search for pair production of heavy vector-like quarks decaying into high-*p_T *W bosons and top quarks in the lepton-plus-jets final state in pp collisions at* $\sqrt{s} = 13$ *TeV with the ATLAS detector*, *JHEP* **08** (2018) 048 [arXiv:1806.01762] [INSPIRE].

JHEP12(2021)106

The CMS collaboration

Yerevan Physics Institute, Yerevan, Armenia

A.M. Sirunyan[†], A. Tumasyan

Institut für Hochenergiephysik, Wien, Austria

W. Adam, T. Bergauer, M. Dragicevic, A. Escalante Del Valle, R. Frühwirth[1], M. Jeitler[1], N. Krammer, L. Lechner, D. Liko, I. Mikulec, F.M. Pitters, J. Schieck[1], R. Schöfbeck, M. Spanring, S. Templ, W. Waltenberger, C.-E. Wulz[1], M. Zarucki

Institute for Nuclear Problems, Minsk, Belarus

V. Chekhovsky, A. Litomin, V. Makarenko

Universiteit Antwerpen, Antwerpen, Belgium

M.R. Darwish[2], E.A. De Wolf, X. Janssen, T. Kello[3], A. Lelek, H. Rejeb Sfar, P. Van Mechelen, S. Van Putte, N. Van Remortel

Vrije Universiteit Brussel, Brussel, Belgium

F. Blekman, E.S. Bols, J. D'Hondt, J. De Clercq, S. Lowette, S. Moortgat, A. Morton, D. Müller, A.R. Sahasransu, S. Tavernier, W. Van Doninck, P. Van Mulders

Université Libre de Bruxelles, Bruxelles, Belgium

D. Beghin, B. Bilin, B. Clerbaux, G. De Lentdecker, B. Dorney, L. Favart, A. Grebenyuk, A.K. Kalsi, K. Lee, I. Makarenko, L. Moureaux, L. Pétré, A. Popov, N. Postiau, E. Starling, L. Thomas, C. Vander Velde, P. Vanlaer, D. Vannerom, L. Wezenbeek

Ghent University, Ghent, Belgium

T. Cornelis, D. Dobur, M. Gruchala, I. Khvastunov[4], G. Mestdach, M. Niedziela, C. Roskas, K. Skovpen, M. Tytgat, W. Verbeke, B. Vermassen, M. Vit

Université Catholique de Louvain, Louvain-la-Neuve, Belgium

A. Bethani, G. Bruno, F. Bury, C. Caputo, P. David, C. Delaere, M. Delcourt, I.S. Donertas, A. Giammanco, V. Lemaitre, K. Mondal, J. Prisciandaro, A. Taliercio, M. Teklishyn, P. Vischia, S. Wertz, S. Wuyckens

Centro Brasileiro de Pesquisas Fisicas, Rio de Janeiro, Brazil

G.A. Alves, C. Hensel, A. Moraes

Universidade do Estado do Rio de Janeiro, Rio de Janeiro, Brazil

W.L. Aldá Júnior, E. Belchior Batista Das Chagas, H. Brandao Malbouisson, W. Carvalho, J. Chinellato[5], E. Coelho, E.M. Da Costa, G.G. Da Silveira[6], D. De Jesus Damiao, S. Fonseca De Souza, J. Martins[7], D. Matos Figueiredo, C. Mora Herrera, L. Mundim, H. Nogima, P. Rebello Teles, L.J. Sanchez Rosas, A. Santoro, S.M. Silva Do Amaral, A. Sznajder, M. Thiel, F. Torres Da Silva De Araujo, A. Vilela Pereira

Universidade Estadual Paulista [a], Universidade Federal do ABC [b], São Paulo, Brazil

C.A. Bernardes[a], L. Calligaris[a], T.R. Fernandez Perez Tomei[a], E.M. Gregores[a,b], D.S. Lemos[a], P.G. Mercadante[a,b], S.F. Novaes[a], S.S. Padula[a]

JHEP12(2021)106

Institute for Nuclear Research and Nuclear Energy, Bulgarian Academy of Sciences, Sofia, Bulgaria
A. Aleksandrov, G. Antchev, I. Atanasov, R. Hadjiiska, P. Iaydjiev, M. Misheva, M. Rodozov, M. Shopova, G. Sultanov

University of Sofia, Sofia, Bulgaria
A. Dimitrov, T. Ivanov, L. Litov, B. Pavlov, P. Petkov, A. Petrov

Beihang University, Beijing, China
T. Cheng, W. Fang[3], Q. Guo, M. Mittal, H. Wang, L. Yuan

Department of Physics, Tsinghua University, Beijing, China
M. Ahmad, G. Bauer, Z. Hu, Y. Wang, K. Yi[8,9]

Institute of High Energy Physics, Beijing, China
E. Chapon, G.M. Chen[10], H.S. Chen[10], M. Chen, T. Javaid[10], A. Kapoor, D. Leggat, H. Liao, Z.-A. LIU[10], R. Sharma, A. Spiezia, J. Tao, J. Thomas-Wilsker, J. Wang, H. Zhang, S. Zhang[10], J. Zhao

State Key Laboratory of Nuclear Physics and Technology, Peking University, Beijing, China
A. Agapitos, Y. Ban, C. Chen, Q. Huang, A. Levin, Q. Li, M. Lu, X. Lyu, Y. Mao, S.J. Qian, D. Wang, Q. Wang, J. Xiao

Sun Yat-Sen University, Guangzhou, China
Z. You

Institute of Modern Physics and Key Laboratory of Nuclear Physics and Ion-beam Application (MOE) — Fudan University, Shanghai, China
X. Gao[3], H. Okawa

Zhejiang University, Hangzhou, China
M. Xiao

Universidad de Los Andes, Bogota, Colombia
C. Avila, A. Cabrera, C. Florez, J. Fraga, A. Sarkar, M.A. Segura Delgado

Universidad de Antioquia, Medellin, Colombia
J. Jaramillo, J. Mejia Guisao, F. Ramirez, J.D. Ruiz Alvarez, C.A. Salazar González, N. Vanegas Arbelaez

University of Split, Faculty of Electrical Engineering, Mechanical Engineering and Naval Architecture, Split, Croatia
D. Giljanovic, N. Godinovic, D. Lelas, I. Puljak

University of Split, Faculty of Science, Split, Croatia
Z. Antunovic, M. Kovac, T. Sculac

Institute Rudjer Boskovic, Zagreb, Croatia
V. Brigljevic, D. Ferencek, D. Majumder, M. Roguljic, A. Starodumov[11], T. Susa

JHEP12(2021)106

University of Cyprus, Nicosia, Cyprus

M.W. Ather, A. Attikis, E. Erodotou, A. Ioannou, G. Kole, M. Kolosova, S. Konstantinou, J. Mousa, C. Nicolaou, F. Ptochos, P.A. Razis, H. Rykaczewski, H. Saka, D. Tsiakkouri

Charles University, Prague, Czech Republic

M. Finger[12], M. Finger Jr.[12], A. Kveton, J. Tomsa

Escuela Politecnica Nacional, Quito, Ecuador

E. Ayala

Universidad San Francisco de Quito, Quito, Ecuador

E. Carrera Jarrin

Academy of Scientific Research and Technology of the Arab Republic of Egypt, Egyptian Network of High Energy Physics, Cairo, Egypt

H. Abdalla[13], Y. Assran[14,15], E. Salama[15,16]

Center for High Energy Physics (CHEP-FU), Fayoum University, El-Fayoum, Egypt

A. Lotfy, M.A. Mahmoud

National Institute of Chemical Physics and Biophysics, Tallinn, Estonia

S. Bhowmik, A. Carvalho Antunes De Oliveira, R.K. Dewanjee, K. Ehataht, M. Kadastik, J. Pata, M. Raidal, C. Veelken

Department of Physics, University of Helsinki, Helsinki, Finland

P. Eerola, L. Forthomme, H. Kirschenmann, K. Osterberg, M. Voutilainen

Helsinki Institute of Physics, Helsinki, Finland

E. Brücken, F. Garcia, J. Havukainen, V. Karimäki, M.S. Kim, R. Kinnunen, T. Lampén, K. Lassila-Perini, S. Lehti, T. Lindén, H. Siikonen, E. Tuominen, J. Tuominiemi

Lappeenranta University of Technology, Lappeenranta, Finland

P. Luukka, T. Tuuva

IRFU, CEA, Université Paris-Saclay, Gif-sur-Yvette, France

C. Amendola, M. Besancon, F. Couderc, M. Dejardin, D. Denegri, J.L. Faure, F. Ferri, S. Ganjour, A. Givernaud, P. Gras, G. Hamel de Monchenault, P. Jarry, B. Lenzi, E. Locci, J. Malcles, J. Rander, A. Rosowsky, M.Ö. Sahin, A. Savoy-Navarro[17], M. Titov, G.B. Yu

Laboratoire Leprince-Ringuet, CNRS/IN2P3, Ecole Polytechnique, Institut Polytechnique de Paris, Palaiseau, France

S. Ahuja, F. Beaudette, M. Bonanomi, A. Buchot Perraguin, P. Busson, C. Charlot, O. Davignon, B. Diab, G. Falmagne, R. Granier de Cassagnac, A. Hakimi, I. Kucher, A. Lobanov, C. Martin Perez, M. Nguyen, C. Ochando, P. Paganini, J. Rembser, R. Salerno, J.B. Sauvan, Y. Sirois, A. Zabi, A. Zghiche

JHEP12(2021)106

Université de Strasbourg, CNRS, IPHC UMR 7178, Strasbourg, France

J.-L. Agram[18], J. Andrea, D. Apparu, D. Bloch, G. Bourgatte, J.-M. Brom, E.C. Chabert, C. Collard, D. Darej, J.-C. Fontaine[18], U. Goerlach, C. Grimault, A.-C. Le Bihan, P. Van Hove

Institut de Physique des 2 Infinis de Lyon (IP2I), Villeurbanne, France

E. Asilar, S. Beauceron, C. Bernet, G. Boudoul, C. Camen, A. Carle, N. Chanon, D. Contardo, P. Depasse, H. El Mamouni, J. Fay, S. Gascon, M. Gouzevitch, B. Ille, Sa. Jain, I.B. Laktineh, H. Lattaud, A. Lesauvage, M. Lethuillier, L. Mirabito, K. Shchablo, L. Torterotot, G. Touquet, M. Vander Donckt, S. Viret

Georgian Technical University, Tbilisi, Georgia

A. Khvedelidze[12], Z. Tsamalaidze[12]

RWTH Aachen University, I. Physikalisches Institut, Aachen, Germany

L. Feld, K. Klein, M. Lipinski, D. Meuser, A. Pauls, M.P. Rauch, J. Schulz, M. Teroerde

RWTH Aachen University, III. Physikalisches Institut A, Aachen, Germany

D. Eliseev, M. Erdmann, P. Fackeldey, B. Fischer, S. Ghosh, T. Hebbeker, K. Hoepfner, H. Keller, L. Mastrolorenzo, M. Merschmeyer, A. Meyer, G. Mocellin, S. Mondal, S. Mukherjee, D. Noll, A. Novak, T. Pook, A. Pozdnyakov, Y. Rath, H. Reithler, J. Roemer, A. Schmidt, S.C. Schuler, A. Sharma, S. Wiedenbeck, S. Zaleski

RWTH Aachen University, III. Physikalisches Institut B, Aachen, Germany

C. Dziwok, G. Flügge, W. Haj Ahmad[19], O. Hlushchenko, T. Kress, A. Nowack, C. Pistone, O. Pooth, D. Roy, H. Sert, A. Stahl[20], T. Ziemons

Deutsches Elektronen-Synchrotron, Hamburg, Germany

H. Aarup Petersen, M. Aldaya Martin, P. Asmuss, I. Babounikau, S. Baxter, O. Behnke, A. Bermúdez Martínez, A.A. Bin Anuar, K. Borras[21], V. Botta, D. Brunner, A. Campbell, A. Cardini, P. Connor, S. Consuegra Rodríguez, V. Danilov, M.M. Defranchis, L. Didukh, D. Domínguez Damiani, G. Eckerlin, D. Eckstein, L.I. Estevez Banos, E. Gallo[22], A. Geiser, A. Giraldi, A. Grohsjean, M. Guthoff, A. Harb, A. Jafari[23], N.Z. Jomhari, H. Jung, A. Kasem[21], M. Kasemann, H. Kaveh, C. Kleinwort, J. Knolle, D. Krücker, W. Lange, T. Lenz, J. Lidrych, K. Lipka, W. Lohmann[24], T. Madlener, R. Mankel, I.-A. Melzer-Pellmann, J. Metwally, A.B. Meyer, M. Meyer, J. Mnich, A. Mussgiller, V. Myronenko, Y. Otarid, D. Pérez Adán, S.K. Pflitsch, D. Pitzl, A. Raspereza, A. Saggio, A. Saibel, M. Savitskyi, V. Scheurer, C. Schwanenberger, A. Singh, R.E. Sosa Ricardo, N. Tonon, O. Turkot, A. Vagnerini, M. Van De Klundert, R. Walsh, D. Walter, Y. Wen, K. Wichmann, C. Wissing, S. Wuchterl, O. Zenaiev, R. Zlebcik

University of Hamburg, Hamburg, Germany

R. Aggleton, S. Bein, L. Benato, A. Benecke, K. De Leo, T. Dreyer, M. Eich, F. Feindt, A. Fröhlich, C. Garbers, E. Garutti, P. Gunnellini, J. Haller, A. Hinzmann, A. Karavdina, G. Kasieczka, R. Klanner, R. Kogler, V. Kutzner, J. Lange, T. Lange, A. Malara, C.E.N. Niemeyer, A. Nigamova, K.J. Pena Rodriguez, O. Rieger, P. Schleper, M. Schröder,

JHEP12(2021)106

J. Schwandt, D. Schwarz, J. Sonneveld, H. Stadie, G. Steinbrück, A. Tews, B. Vormwald, I. Zoi

Karlsruher Institut fuer Technologie, Karlsruhe, Germany

J. Bechtel, T. Berger, E. Butz, R. Caspart, T. Chwalek, W. De Boer, A. Dierlamm, A. Droll, K. El Morabit, N. Faltermann, K. Flöh, M. Giffels, J.o. Gosewisch, A. Gottmann, F. Hartmann[20], C. Heidecker, U. Husemann, I. Katkov[25], P. Keicher, R. Koppenhöfer, S. Maier, M. Metzler, S. Mitra, Th. Müller, M. Musich, M. Neukum, G. Quast, K. Rabbertz, J. Rauser, D. Savoiu, D. Schäfer, M. Schnepf, D. Seith, I. Shvetsov, H.J. Simonis, R. Ulrich, J. Van Der Linden, R.F. Von Cube, M. Wassmer, M. Weber, S. Wieland, R. Wolf, S. Wozniewski, S. Wunsch

Institute of Nuclear and Particle Physics (INPP), NCSR Demokritos, Aghia Paraskevi, Greece

G. Anagnostou, P. Asenov, G. Daskalakis, T. Geralis, A. Kyriakis, D. Loukas, G. Paspalaki, A. Stakia

National and Kapodistrian University of Athens, Athens, Greece

M. Diamantopoulou, D. Karasavvas, G. Karathanasis, P. Kontaxakis, C.K. Koraka, A. Manousakis-Katsikakis, A. Panagiotou, I. Papavergou, N. Saoulidou, K. Theofilatos, E. Tziaferi, K. Vellidis, E. Vourliotis

National Technical University of Athens, Athens, Greece

G. Bakas, K. Kousouris, I. Papakrivopoulos, G. Tsipolitis, A. Zacharopoulou

University of Ioánnina, Ioánnina, Greece

I. Evangelou, C. Foudas, P. Gianneios, P. Katsoulis, P. Kokkas, N. Manthos, I. Papadopoulos, J. Strologas

MTA-ELTE Lendület CMS Particle and Nuclear Physics Group, Eötvös Loránd University, Budapest, Hungary

M. Csanad, M.M.A. Gadallah[26], S. Lökös[27], P. Major, K. Mandal, A. Mehta, G. Pasztor, O. Surányi, G.I. Veres

Wigner Research Centre for Physics, Budapest, Hungary

M. Bartók[28], G. Bencze, C. Hajdu, D. Horvath[29], F. Sikler, V. Veszpremi, G. Vesztergombi[†]

Institute of Nuclear Research ATOMKI, Debrecen, Hungary

S. Czellar, J. Karancsi[28], J. Molnar, Z. Szillasi, D. Teyssier

Institute of Physics, University of Debrecen, Debrecen, Hungary

P. Raics, Z.L. Trocsanyi[30], B. Ujvari

Eszterhazy Karoly University, Karoly Robert Campus, Gyongyos, Hungary

T. Csorgo[31], F. Nemes[31], T. Novak

Indian Institute of Science (IISc), Bangalore, India

S. Choudhury, J.R. Komaragiri, D. Kumar, L. Panwar, P.C. Tiwari

JHEP12(2021)106

National Institute of Science Education and Research, HBNI, Bhubaneswar, India

S. Bahinipati[32], D. Dash, C. Kar, P. Mal, T. Mishra, V.K. Muraleedharan Nair Bindhu[33], A. Nayak[33], N. Sur, S.K. Swain

Panjab University, Chandigarh, India

S. Bansal, S.B. Beri, V. Bhatnagar, G. Chaudhary, S. Chauhan, N. Dhingra[34], R. Gupta, A. Kaur, S. Kaur, P. Kumari, M. Meena, K. Sandeep, J.B. Singh, A.K. Virdi

University of Delhi, Delhi, India

A. Ahmed, A. Bhardwaj, B.C. Choudhary, R.B. Garg, M. Gola, S. Keshri, A. Kumar, M. Naimuddin, P. Priyanka, K. Ranjan, A. Shah

Saha Institute of Nuclear Physics, HBNI, Kolkata, India

M. Bharti[35], R. Bhattacharya, S. Bhattacharya, D. Bhowmik, S. Dutta, S. Ghosh, B. Gomber[36], M. Maity[37], S. Nandan, P. Palit, P.K. Rout, G. Saha, B. Sahu, S. Sarkar, M. Sharan, B. Singh[35], S. Thakur[35]

Indian Institute of Technology Madras, Madras, India

P.K. Behera, S.C. Behera, P. Kalbhor, A. Muhammad, R. Pradhan, P.R. Pujahari, A. Sharma, A.K. Sikdar

Bhabha Atomic Research Centre, Mumbai, India

D. Dutta, V. Jha, V. Kumar, D.K. Mishra, K. Naskar[38], P.K. Netrakanti, L.M. Pant, P. Shukla

Tata Institute of Fundamental Research-A, Mumbai, India

T. Aziz, S. Dugad, G.B. Mohanty, U. Sarkar

Tata Institute of Fundamental Research-B, Mumbai, India

S. Banerjee, S. Bhattacharya, S. Chatterjee, R. Chudasama, M. Guchait, S. Karmakar, S. Kumar, G. Majumder, K. Mazumdar, S. Mukherjee, D. Roy

Indian Institute of Science Education and Research (IISER), Pune, India

S. Dube, B. Kansal, S. Pandey, A. Rane, A. Rastogi, S. Sharma

Department of Physics, Isfahan University of Technology, Isfahan, Iran

H. Bakhshiansohi[39], M. Zeinali[40]

Institute for Research in Fundamental Sciences (IPM), Tehran, Iran

S. Chenarani[41], S.M. Etesami, M. Khakzad, M. Mohammadi Najafabadi

University College Dublin, Dublin, Ireland

M. Felcini, M. Grunewald

INFN Sezione di Bari [a], Università di Bari [b], Politecnico di Bari [c], Bari, Italy

M. Abbrescia[a,b], R. Aly[a,b,42], C. Aruta[a,b], A. Colaleo[a], D. Creanza[a,c], N. De Filippis[a,c], M. De Palma[a,b], A. Di Florio[a,b], A. Di Pilato[a,b], W. Elmetenawee[a,b], L. Fiore[a], A. Gelmi[a,b], M. Gul[a], G. Iaselli[a,c], M. Ince[a,b], S. Lezki[a,b], G. Maggi[a,c], M. Maggi[a], I. Margjeka[a,b],

JHEP12(2021)106

V. Mastrapasqua[a,b], J.A. Merlin[a], S. My[a,b], S. Nuzzo[a,b], A. Pompili[a,b], G. Pugliese[a,c], A. Ranieri[a], G. Selvaggi[a,b], L. Silvestris[a], F.M. Simone[a,b], R. Venditti[a], P. Verwilligen[a]

INFN Sezione di Bologna [a], Università di Bologna [b], Bologna, Italy

G. Abbiendi[a], C. Battilana[a,b], D. Bonacorsi[a,b], L. Borgonovi[a], S. Braibant-Giacomelli[a,b], R. Campanini[a,b], P. Capiluppi[a,b], A. Castro[a,b], F.R. Cavallo[a], C. Ciocca[a], M. Cuffiani[a,b], G.M. Dallavalle[a], T. Diotalevi[a,b], F. Fabbri[a], A. Fanfani[a,b], E. Fontanesi[a,b], P. Giacomelli[a], L. Giommi[a,b], C. Grandi[a], L. Guiducci[a,b], F. Iemmi[a,b], S. Lo Meo[a,43], S. Marcellini[a], G. Masetti[a], F.L. Navarria[a,b], A. Perrotta[a], F. Primavera[a,b], A.M. Rossi[a,b], T. Rovelli[a,b], G.P. Siroli[a,b], N. Tosi[a]

INFN Sezione di Catania [a], Università di Catania [b], Catania, Italy

S. Albergo[a,b,44], S. Costa[a,b,44], A. Di Mattia[a], R. Potenza[a,b], A. Tricomi[a,b,44], C. Tuve[a,b]

INFN Sezione di Firenze [a], Università di Firenze [b], Firenze, Italy

G. Barbagli[a], A. Cassese[a], R. Ceccarelli[a,b], V. Ciulli[a,b], C. Civinini[a], R. D'Alessandro[a,b], F. Fiori[a], E. Focardi[a,b], G. Latino[a,b], P. Lenzi[a,b], M. Lizzo[a,b], M. Meschini[a], S. Paoletti[a], R. Seidita[a,b], G. Sguazzoni[a], L. Viliani[a]

INFN Laboratori Nazionali di Frascati, Frascati, Italy

L. Benussi, S. Bianco, D. Piccolo

INFN Sezione di Genova [a], Università di Genova [b], Genova, Italy

M. Bozzo[a,b], F. Ferro[a], R. Mulargia[a,b], E. Robutti[a], S. Tosi[a,b]

INFN Sezione di Milano-Bicocca [a], Università di Milano-Bicocca [b], Milano, Italy

A. Benaglia[a], A. Beschi[a,b], F. Brivio[a,b], F. Cetorelli[a,b], V. Ciriolo[a,b,20], F. De Guio[a,b], M.E. Dinardo[a,b], P. Dini[a], S. Gennai[a], A. Ghezzi[a,b], P. Govoni[a,b], L. Guzzi[a,b], M. Malberti[a], S. Malvezzi[a], A. Massironi[a], D. Menasce[a], F. Monti[a,b], L. Moroni[a], M. Paganoni[a,b], D. Pedrini[a], S. Ragazzi[a,b], T. Tabarelli de Fatis[a,b], D. Valsecchi[a,b,20], D. Zuolo[a,b]

INFN Sezione di Napoli [a], Università di Napoli 'Federico II' [b], Napoli, Italy, Università della Basilicata [c], Potenza, Italy, Università G. Marconi [d], Roma, Italy

S. Buontempo[a], N. Cavallo[a,c], A. De Iorio[a,b], F. Fabozzi[a,c], F. Fienga[a], A.O.M. Iorio[a,b], L. Lista[a,b], S. Meola[a,d,20], P. Paolucci[a,20], B. Rossi[a], C. Sciacca[a,b]

INFN Sezione di Padova [a], Università di Padova [b], Padova, Italy, Università di Trento [c], Trento, Italy

P. Azzi[a], N. Bacchetta[a], D. Bisello[a,b], P. Bortignon[a], A. Bragagnolo[a,b], R. Carlin[a,b], P. Checchia[a], P. De Castro Manzano[a], T. Dorigo[a], F. Gasparini[a,b], U. Gasparini[a,b], S.Y. Hoh[a,b], L. Layer[a,45], M. Margoni[a,b], A.T. Meneguzzo[a,b], M. Presilla[a,b], P. Ronchese[a,b], R. Rossin[a,b], F. Simonetto[a,b], G. Strong[a], M. Tosi[a,b], H. Yarar[a,b], M. Zanetti[a,b], P. Zotto[a,b], A. Zucchetta[a,b], G. Zumerle[a,b]

JHEP12(2021)106

INFN Sezione di Pavia [a], Università di Pavia [b], Pavia, Italy

C. Aime'[a,b], A. Braghieri[a], S. Calzaferri[a,b], D. Fiorina[a,b], P. Montagna[a,b], S.P. Ratti[a,b], V. Re[a], M. Ressegotti[a,b], C. Riccardi[a,b], P. Salvini[a], I. Vai[a], P. Vitulo[a,b]

INFN Sezione di Perugia [a], Università di Perugia [b], Perugia, Italy

G.M. Bilei[a], D. Ciangottini[a,b], L. Fanò[a,b], P. Lariccia[a,b], G. Mantovani[a,b], V. Mariani[a,b], M. Menichelli[a], F. Moscatelli[a], A. Piccinelli[a,b], A. Rossi[a,b], A. Santocchia[a,b], D. Spiga[a], T. Tedeschi[a,b]

INFN Sezione di Pisa [a], Università di Pisa [b], Scuola Normale Superiore di Pisa [c], Pisa Italy, Università di Siena [d], Siena, Italy

K. Androsov[a], P. Azzurri[a], G. Bagliesi[a], V. Bertacchi[a,c], L. Bianchini[a], T. Boccali[a], E. Bossini, R. Castaldi[a], M.A. Ciocci[a,b], R. Dell'Orso[a], M.R. Di Domenico[a,d], S. Donato[a], A. Giassi[a], M.T. Grippo[a], F. Ligabue[a,c], E. Manca[a,c], G. Mandorli[a,c], A. Messineo[a,b], F. Palla[a], G. Ramirez-Sanchez[a,c], A. Rizzi[a,b], G. Rolandi[a,c], S. Roy Chowdhury[a,c], A. Scribano[a], N. Shafiei[a,b], P. Spagnolo[a], R. Tenchini[a], G. Tonelli[a,b], N. Turini[a,d], A. Venturi[a], P.G. Verdini[a]

INFN Sezione di Roma [a], Sapienza Università di Roma [b], Rome, Italy

F. Cavallari[a], M. Cipriani[a,b], D. Del Re[a,b], E. Di Marco[a], M. Diemoz[a], E. Longo[a,b], P. Meridiani[a], G. Organtini[a,b], F. Pandolfi[a], R. Paramatti[a,b], C. Quaranta[a,b], S. Rahatlou[a,b], C. Rovelli[a], F. Santanastasio[a,b], L. Soffi[a,b], R. Tramontano[a,b]

INFN Sezione di Torino [a], Università di Torino [b], Torino, Italy, Università del Piemonte Orientale [c], Novara, Italy

N. Amapane[a,b], R. Arcidiacono[a,c], S. Argiro[a,b], M. Arneodo[a,c], N. Bartosik[a], R. Bellan[a,b], A. Bellora[a,b], J. Berenguer Antequera[a,b], C. Biino[a], A. Cappati[a,b], N. Cartiglia[a], S. Cometti[a], M. Costa[a,b], R. Covarelli[a,b], N. Demaria[a], B. Kiani[a,b], F. Legger[a], C. Mariotti[a], S. Maselli[a], E. Migliore[a,b], V. Monaco[a,b], E. Monteil[a,b], M. Monteno[a], M.M. Obertino[a,b], G. Ortona[a], L. Pacher[a,b], N. Pastrone[a], M. Pelliccioni[a], G.L. Pinna Angioni[a,b], M. Ruspa[a,c], R. Salvatico[a,b], F. Siviero[a,b], V. Sola[a], A. Solano[a,b], D. Soldi[a,b], A. Staiano[a], M. Tornago[a,b], D. Trocino[a,b]

INFN Sezione di Trieste [a], Università di Trieste [b], Trieste, Italy

S. Belforte[a], V. Candelise[a,b], M. Casarsa[a], F. Cossutti[a], A. Da Rold[a,b], G. Della Ricca[a,b], F. Vazzoler[a,b]

Kyungpook National University, Daegu, Korea

S. Dogra, C. Huh, B. Kim, D.H. Kim, G.N. Kim, J. Lee, S.W. Lee, C.S. Moon, Y.D. Oh, S.I. Pak, B.C. Radburn-Smith, S. Sekmen, Y.C. Yang

Chonnam National University, Institute for Universe and Elementary Particles, Kwangju, Korea

H. Kim, D.H. Moon

Hanyang University, Seoul, Korea

B. Francois, T.J. Kim, J. Park

JHEP12(2021)106

Korea University, Seoul, Korea
S. Cho, S. Choi, Y. Go, B. Hong, K. Lee, K.S. Lee, J. Lim, J. Park, S.K. Park, J. Yoo

Kyung Hee University, Department of Physics, Seoul, Republic of Korea
J. Goh, A. Gurtu

Sejong University, Seoul, Korea
H.S. Kim, Y. Kim

Seoul National University, Seoul, Korea
J. Almond, J.H. Bhyun, J. Choi, S. Jeon, J. Kim, J.S. Kim, S. Ko, H. Kwon, H. Lee, S. Lee, K. Nam, B.H. Oh, M. Oh, S.B. Oh, H. Seo, U.K. Yang, I. Yoon

University of Seoul, Seoul, Korea
D. Jeon, J.H. Kim, B. Ko, J.S.H. Lee, I.C. Park, Y. Roh, D. Song, I.J. Watson

Yonsei University, Department of Physics, Seoul, Korea
S. Ha, H.D. Yoo

Sungkyunkwan University, Suwon, Korea
Y. Choi, C. Hwang, Y. Jeong, H. Lee, Y. Lee, I. Yu

College of Engineering and Technology, American University of the Middle East (AUM), Egaila, Kuwait
Y. Maghrbi

Riga Technical University, Riga, Latvia
V. Veckalns[46]

Vilnius University, Vilnius, Lithuania
M. Ambrozas, A. Juodagalvis, A. Rinkevicius, G. Tamulaitis, A. Vaitkevicius

National Centre for Particle Physics, Universiti Malaya, Kuala Lumpur, Malaysia
W.A.T. Wan Abdullah, M.N. Yusli, Z. Zolkapli

Universidad de Sonora (UNISON), Hermosillo, Mexico
J.F. Benitez, A. Castaneda Hernandez, J.A. Murillo Quijada, L. Valencia Palomo

Centro de Investigacion y de Estudios Avanzados del IPN, Mexico City, Mexico
G. Ayala, H. Castilla-Valdez, E. De La Cruz-Burelo, I. Heredia-De La Cruz[47], R. Lopez-Fernandez, C.A. Mondragon Herrera, D.A. Perez Navarro, A. Sanchez-Hernandez

Universidad Iberoamericana, Mexico City, Mexico
S. Carrillo Moreno, C. Oropeza Barrera, M. Ramirez-Garcia, F. Vazquez Valencia

Benemerita Universidad Autonoma de Puebla, Puebla, Mexico
I. Pedraza, H.A. Salazar Ibarguen, C. Uribe Estrada

University of Montenegro, Podgorica, Montenegro
J. Mijuskovic[4], N. Raicevic

JHEP12(2021)106

University of Auckland, Auckland, New Zealand
D. Krofcheck

University of Canterbury, Christchurch, New Zealand
S. Bheesette, P.H. Butler

National Centre for Physics, Quaid-I-Azam University, Islamabad, Pakistan
A. Ahmad, M.I. Asghar, A. Awais, M.I.M. Awan, H.R. Hoorani, W.A. Khan, M.A. Shah, M. Shoaib, M. Waqas

AGH University of Science and Technology Faculty of Computer Science, Electronics and Telecommunications, Krakow, Poland
V. Avati, L. Grzanka, M. Malawski

National Centre for Nuclear Research, Swierk, Poland
H. Bialkowska, M. Bluj, B. Boimska, T. Frueboes, M. Górski, M. Kazana, M. Szleper, P. Traczyk, P. Zalewski

Institute of Experimental Physics, Faculty of Physics, University of Warsaw, Warsaw, Poland
K. Bunkowski, K. Doroba, A. Kalinowski, M. Konecki, J. Krolikowski, M. Walczak

Laboratório de Instrumentação e Física Experimental de Partículas, Lisboa, Portugal
M. Araujo, P. Bargassa, D. Bastos, A. Boletti, P. Faccioli, M. Gallinaro, J. Hollar, N. Leonardo, T. Niknejad, J. Seixas, K. Shchelina, O. Toldaiev, J. Varela

Joint Institute for Nuclear Research, Dubna, Russia
S. Afanasiev, D. Budkouski, P. Bunin, M. Gavrilenko, I. Golutvin, I. Gorbunov, A. Kamenev, V. Karjavine, A. Lanev, A. Malakhov, V. Matveev[48,49], V. Palichik, V. Perelygin, M. Savina, D. Seitova, V. Shalaev, S. Shmatov, S. Shulha, V. Smirnov, O. Teryaev, N. Voytishin, A. Zarubin, I. Zhizhin

Petersburg Nuclear Physics Institute, Gatchina (St. Petersburg), Russia
G. Gavrilov, V. Golovtcov, Y. Ivanov, V. Kim[50], E. Kuznetsova[51], V. Murzin, V. Oreshkin, I. Smirnov, D. Sosnov, V. Sulimov, L. Uvarov, S. Volkov, A. Vorobyev

Institute for Nuclear Research, Moscow, Russia
Yu. Andreev, A. Dermenev, S. Gninenko, N. Golubev, A. Karneyeu, M. Kirsanov, N. Krasnikov, A. Pashenkov, G. Pivovarov, D. Tlisov†, A. Toropin

Institute for Theoretical and Experimental Physics named by A.I. Alikhanov of NRC 'Kurchatov Institute', Moscow, Russia
V. Epshteyn, V. Gavrilov, N. Lychkovskaya, A. Nikitenko[52], V. Popov, G. Safronov, A. Spiridonov, A. Stepennov, M. Toms, E. Vlasov, A. Zhokin

Moscow Institute of Physics and Technology, Moscow, Russia
T. Aushev

JHEP12(2021)106

National Research Nuclear University 'Moscow Engineering Physics Institute' (MEPhI), Moscow, Russia

R. Chistov[53], M. Danilov[54], A. Oskin, P. Parygin, S. Polikarpov[53]

P.N. Lebedev Physical Institute, Moscow, Russia

V. Andreev, M. Azarkin, I. Dremin, M. Kirakosyan, A. Terkulov

Skobeltsyn Institute of Nuclear Physics, Lomonosov Moscow State University, Moscow, Russia

A. Belyaev, E. Boos, V. Bunichev, M. Dubinin[55], L. Dudko, V. Klyukhin, O. Kodolova, I. Lokhtin, S. Obraztsov, M. Perfilov, S. Petrushanko, V. Savrin, P. Volkov

Novosibirsk State University (NSU), Novosibirsk, Russia

V. Blinov[56], T. Dimova[56], L. Kardapoltsev[56], I. Ovtin[56], Y. Skovpen[56]

Institute for High Energy Physics of National Research Centre 'Kurchatov Institute', Protvino, Russia

I. Azhgirey, I. Bayshev, V. Kachanov, A. Kalinin, D. Konstantinov, V. Petrov, R. Ryutin, A. Sobol, S. Troshin, N. Tyurin, A. Uzunian, A. Volkov

National Research Tomsk Polytechnic University, Tomsk, Russia

A. Babaev, A. Iuzhakov, V. Okhotnikov, L. Sukhikh

Tomsk State University, Tomsk, Russia

V. Borchsh, V. Ivanchenko, E. Tcherniaev

University of Belgrade: Faculty of Physics and VINCA Institute of Nuclear Sciences, Belgrade, Serbia

P. Adzic[57], M. Dordevic, P. Milenovic, J. Milosevic

Centro de Investigaciones Energéticas Medioambientales y Tecnológicas (CIEMAT), Madrid, Spain

M. Aguilar-Benitez, J. Alcaraz Maestre, A. Álvarez Fernández, I. Bachiller, M. Barrio Luna, Cristina F. Bedoya, C.A. Carrillo Montoya, M. Cepeda, M. Cerrada, N. Colino, B. De La Cruz, A. Delgado Peris, J.P. Fernández Ramos, J. Flix, M.C. Fouz, O. Gonzalez Lopez, S. Goy Lopez, J.M. Hernandez, M.I. Josa, J. León Holgado, D. Moran, Á. Navarro Tobar, A. Pérez-Calero Yzquierdo, J. Puerta Pelayo, I. Redondo, L. Romero, S. Sánchez Navas, M.S. Soares, L. Urda Gómez, C. Willmott

Universidad Autónoma de Madrid, Madrid, Spain

C. Albajar, J.F. de Trocóniz, R. Reyes-Almanza

Universidad de Oviedo, Instituto Universitario de Ciencias y Tecnologías Espaciales de Asturias (ICTEA), Oviedo, Spain

B. Alvarez Gonzalez, J. Cuevas, C. Erice, J. Fernandez Menendez, S. Folgueras, I. Gonzalez Caballero, E. Palencia Cortezon, C. Ramón Álvarez, J. Ripoll Sau, V. Rodríguez Bouza, A. Trapote

JHEP12(2021)106

Instituto de Física de Cantabria (IFCA), CSIC-Universidad de Cantabria, Santander, Spain

J.A. Brochero Cifuentes, I.J. Cabrillo, A. Calderon, B. Chazin Quero, J. Duarte Campderros, M. Fernandez, C. Fernandez Madrazo, P.J. Fernández Manteca, A. García Alonso, G. Gomez, C. Martinez Rivero, P. Martinez Ruiz del Arbol, F. Matorras, J. Piedra Gomez, C. Prieels, F. Ricci-Tam, T. Rodrigo, A. Ruiz-Jimeno, L. Scodellaro, N. Trevisani, I. Vila, J.M. Vizan Garcia

University of Colombo, Colombo, Sri Lanka

M.K. Jayananda, B. Kailasapathy[58], D.U.J. Sonnadara, D.D.C. Wickramarathna

University of Ruhuna, Department of Physics, Matara, Sri Lanka

W.G.D. Dharmaratna, K. Liyanage, N. Perera, N. Wickramage

CERN, European Organization for Nuclear Research, Geneva, Switzerland

T.K. Aarrestad, D. Abbaneo, E. Auffray, G. Auzinger, J. Baechler, P. Baillon, A.H. Ball, D. Barney, J. Bendavid, N. Beni, M. Bianco, A. Bocci, E. Brondolin, T. Camporesi, M. Capeans Garrido, G. Cerminara, S.S. Chhibra, L. Cristella, D. d'Enterria, A. Dabrowski, N. Daci, A. David, A. De Roeck, M. Deile, R. Di Maria, M. Dobson, M. Dünser, N. Dupont, A. Elliott-Peisert, N. Emriskova, F. Fallavollita[59], D. Fasanella, S. Fiorendi, A. Florent, G. Franzoni, J. Fulcher, W. Funk, S. Giani, D. Gigi, K. Gill, F. Glege, L. Gouskos, M. Haranko, J. Hegeman, Y. Iiyama, V. Innocente, T. James, P. Janot, J. Kaspar, J. Kieseler, M. Komm, N. Kratochwil, C. Lange, S. Laurila, P. Lecoq, K. Long, C. Lourenço, L. Malgeri, S. Mallios, M. Mannelli, F. Meijers, S. Mersi, E. Meschi, F. Moortgat, M. Mulders, S. Orfanelli, L. Orsini, F. Pantaleo[20], L. Pape, E. Perez, M. Peruzzi, A. Petrilli, G. Petrucciani, A. Pfeiffer, M. Pierini, M. Pitt, T. Quast, D. Rabady, A. Racz, M. Rieger, M. Rovere, H. Sakulin, J. Salfeld-Nebgen, S. Scarfi, C. Schäfer, C. Schwick, M. Selvaggi, A. Sharma, P. Silva, W. Snoeys, P. Sphicas[60], S. Summers, V.R. Tavolaro, D. Treille, A. Tsirou, G.P. Van Onsem, M. Verzetti, K.A. Wozniak, W.D. Zeuner

Paul Scherrer Institut, Villigen, Switzerland

L. Caminada[61], A. Ebrahimi, W. Erdmann, R. Horisberger, Q. Ingram, H.C. Kaestli, D. Kotlinski, U. Langenegger, M. Missiroli, T. Rohe

ETH Zurich — Institute for Particle Physics and Astrophysics (IPA), Zurich, Switzerland

M. Backhaus, P. Berger, A. Calandri, N. Chernyavskaya, A. De Cosa, G. Dissertori, M. Dittmar, M. Donegà, C. Dorfer, T. Gadek, T.A. Gómez Espinosa, C. Grab, D. Hits, W. Lustermann, A.-M. Lyon, R.A. Manzoni, M.T. Meinhard, F. Micheli, F. Nessi-Tedaldi, J. Niedziela, F. Pauss, V. Perovic, G. Perrin, S. Pigazzini, M.G. Ratti, M. Reichmann, C. Reissel, T. Reitenspiess, B. Ristic, D. Ruini, D.A. Sanz Becerra, M. Schönenberger, V. Stampf, J. Steggemann[62], R. Wallny, D.H. Zhu

Universität Zürich, Zurich, Switzerland

C. Amsler[63], C. Botta, D. Brzhechko, M.F. Canelli, A. De Wit, R. Del Burgo, J.K. Heikkilä, M. Huwiler, A. Jofrehei, B. Kilminster, S. Leontsinis, A. Macchiolo, P. Meiring, V.M. Mikuni,

JHEP12(2021)106

U. Molinatti, I. Neutelings, G. Rauco, A. Reimers, P. Robmann, S. Sanchez Cruz, K. Schweiger, Y. Takahashi

National Central University, Chung-Li, Taiwan

C. Adloff[64], C.M. Kuo, W. Lin, A. Roy, T. Sarkar[37], S.S. Yu

National Taiwan University (NTU), Taipei, Taiwan

L. Ceard, P. Chang, Y. Chao, K.F. Chen, P.H. Chen, W.-S. Hou, Y.y. Li, R.-S. Lu, E. Paganis, A. Psallidas, A. Steen, E. Yazgan, P.r. Yu

Chulalongkorn University, Faculty of Science, Department of Physics, Bangkok, Thailand

B. Asavapibhop, C. Asawatangtrakuldee, N. Srimanobhas

Çukurova University, Physics Department, Science and Art Faculty, Adana, Turkey

F. Boran, S. Damarseckin[65], Z.S. Demiroglu, F. Dolek, C. Dozen[66], I. Dumanoglu[67], E. Eskut, G. Gokbulut, Y. Guler, E. Gurpinar Guler[68], I. Hos[69], C. Isik, E.E. Kangal[70], O. Kara, A. Kayis Topaksu, U. Kiminsu, G. Onengut, K. Ozdemir[71], A. Polatoz, A.E. Simsek, B. Tali[72], U.G. Tok, S. Turkcapar, I.S. Zorbakir, C. Zorbilmez

Middle East Technical University, Physics Department, Ankara, Turkey

B. Isildak[73], G. Karapinar[74], K. Ocalan[75], M. Yalvac[76]

Bogazici University, Istanbul, Turkey

B. Akgun, I.O. Atakisi, E. Gülmez, M. Kaya[77], O. Kaya[78], Ö. Özçelik, S. Tekten[79], E.A. Yetkin[80]

Istanbul Technical University, Istanbul, Turkey

A. Cakir, K. Cankocak[67], Y. Komurcu, S. Sen[81]

Istanbul University, Istanbul, Turkey

F. Aydogmus Sen, S. Cerci[72], B. Kaynak, S. Ozkorucuklu, D. Sunar Cerci[72]

Institute for Scintillation Materials of National Academy of Science of Ukraine, Kharkov, Ukraine

B. Grynyov

National Scientific Center, Kharkov Institute of Physics and Technology, Kharkov, Ukraine

L. Levchuk

University of Bristol, Bristol, United Kingdom

E. Bhal, S. Bologna, J.J. Brooke, A. Bundock, E. Clement, D. Cussans, H. Flacher, J. Goldstein, G.P. Heath, H.F. Heath, L. Kreczko, B. Krikler, S. Paramesvaran, T. Sakuma, S. Seif El Nasr-Storey, V.J. Smith, N. Stylianou[82], J. Taylor, A. Titterton

JHEP12(2021)106

Rutherford Appleton Laboratory, Didcot, United Kingdom
K.W. Bell, A. Belyaev[83], C. Brew, R.M. Brown, D.J.A. Cockerill, K.V. Ellis, K. Harder, S. Harper, J. Linacre, K. Manolopoulos, D.M. Newbold, E. Olaiya, D. Petyt, T. Reis, T. Schuh, C.H. Shepherd-Themistocleous, A. Thea, I.R. Tomalin, T. Williams

Imperial College, London, United Kingdom
R. Bainbridge, P. Bloch, S. Bonomally, J. Borg, S. Breeze, O. Buchmuller, V. Cepaitis, G.S. Chahal[84], D. Colling, P. Dauncey, G. Davies, M. Della Negra, G. Fedi, G. Hall, M.H. Hassanshahi, G. Iles, J. Langford, L. Lyons, A.-M. Magnan, S. Malik, A. Martelli, V. Milosevic, J. Nash[85], V. Palladino, M. Pesaresi, D.M. Raymond, A. Richards, A. Rose, E. Scott, C. Seez, A. Shtipliyski, A. Tapper, K. Uchida, T. Virdee[20], N. Wardle, S.N. Webb, D. Winterbottom, A.G. Zecchinelli

Brunel University, Uxbridge, United Kingdom
J.E. Cole, A. Khan, P. Kyberd, C.K. Mackay, I.D. Reid, L. Teodorescu, S. Zahid

Baylor University, Waco, U.S.A.
S. Abdullin, A. Brinkerhoff, B. Caraway, J. Dittmann, K. Hatakeyama, A.R. Kanuganti, B. McMaster, N. Pastika, S. Sawant, C. Smith, C. Sutantawibul, J. Wilson

Catholic University of America, Washington, DC, U.S.A.
R. Bartek, A. Dominguez, R. Uniyal, A.M. Vargas Hernandez

The University of Alabama, Tuscaloosa, U.S.A.
A. Buccilli, O. Charaf, S.I. Cooper, D. Di Croce, S.V. Gleyzer, C. Henderson, C.U. Perez, P. Rumerio, C. West

Boston University, Boston, U.S.A.
A. Akpinar, A. Albert, D. Arcaro, C. Cosby, Z. Demiragli, D. Gastler, J. Rohlf, K. Salyer, D. Sperka, D. Spitzbart, I. Suarez, S. Yuan, D. Zou

Brown University, Providence, U.S.A.
G. Benelli, B. Burkle, X. Coubez[21], D. Cutts, Y.t. Duh, M. Hadley, U. Heintz, J.M. Hogan[86], K.H.M. Kwok, E. Laird, G. Landsberg, K.T. Lau, J. Lee, J. Luo, M. Narain, S. Sagir[87], E. Usai, W.Y. Wong, X. Yan, D. Yu, W. Zhang

University of California, Davis, Davis, U.S.A.
R. Band, C. Brainerd, R. Breedon, M. Calderon De La Barca Sanchez, M. Chertok, J. Conway, R. Conway, P.T. Cox, R. Erbacher, C. Flores, F. Jensen, O. Kukral, R. Lander, M. Mulhearn, D. Pellett, M. Shi, D. Taylor, M. Tripathi, Y. Yao, F. Zhang

University of California, Los Angeles, U.S.A.
M. Bachtis, R. Cousins, A. Dasgupta, A. Datta, D. Hamilton, J. Hauser, M. Ignatenko, M.A. Iqbal, T. Lam, N. Mccoll, W.A. Nash, S. Regnard, D. Saltzberg, C. Schnaible, B. Stone, V. Valuev

University of California, Riverside, Riverside, U.S.A.
K. Burt, Y. Chen, R. Clare, J.W. Gary, G. Hanson, G. Karapostoli, O.R. Long, N. Manganelli, M. Olmedo Negrete, W. Si, S. Wimpenny, Y. Zhang

JHEP12(2021)106

University of California, San Diego, La Jolla, U.S.A.

J.G. Branson, P. Chang, S. Cittolin, S. Cooperstein, N. Deelen, J. Duarte, R. Gerosa, L. Giannini, D. Gilbert, V. Krutelyov, J. Letts, M. Masciovecchio, S. May, S. Padhi, M. Pieri, V. Sharma, M. Tadel, A. Vartak, F. Würthwein, A. Yagil

University of California, Santa Barbara — Department of Physics, Santa Barbara, U.S.A.

N. Amin, C. Campagnari, M. Citron, A. Dorsett, V. Dutta, J. Incandela, M. Kilpatrick, B. Marsh, H. Mei, A. Ovcharova, H. Qu, M. Quinnan, J. Richman, U. Sarica, D. Stuart, S. Wang

California Institute of Technology, Pasadena, U.S.A.

A. Bornheim, O. Cerri, I. Dutta, J.M. Lawhorn, N. Lu, J. Mao, H.B. Newman, J. Ngadiuba, T.Q. Nguyen, M. Spiropulu, J.R. Vlimant, C. Wang, S. Xie, Z. Zhang, R.Y. Zhu

Carnegie Mellon University, Pittsburgh, U.S.A.

J. Alison, M.B. Andrews, T. Ferguson, T. Mudholkar, M. Paulini, I. Vorobiev

University of Colorado Boulder, Boulder, U.S.A.

J.P. Cumalat, W.T. Ford, E. MacDonald, R. Patel, A. Perloff, K. Stenson, K.A. Ulmer, S.R. Wagner

Cornell University, Ithaca, U.S.A.

J. Alexander, Y. Cheng, J. Chu, D.J. Cranshaw, K. Mcdermott, J. Monroy, J.R. Patterson, D. Quach, A. Ryd, W. Sun, S.M. Tan, Z. Tao, J. Thom, P. Wittich, M. Zientek

Fermi National Accelerator Laboratory, Batavia, U.S.A.

M. Albrow, M. Alyari, G. Apollinari, A. Apresyan, A. Apyan, S. Banerjee, L.A.T. Bauerdick, A. Beretvas, D. Berry, J. Berryhill, P.C. Bhat, K. Burkett, J.N. Butler, A. Canepa, G.B. Cerati, H.W.K. Cheung, F. Chlebana, M. Cremonesi, K.F. Di Petrillo, V.D. Elvira, J. Freeman, Z. Gecse, L. Gray, D. Green, S. Grünendahl, O. Gutsche, R.M. Harris, R. Heller, T.C. Herwig, J. Hirschauer, B. Jayatilaka, S. Jindariani, M. Johnson, U. Joshi, P. Klabbers, T. Klijnsma, B. Klima, M.J. Kortelainen, S. Lammel, D. Lincoln, R. Lipton, T. Liu, J. Lykken, C. Madrid, K. Maeshima, C. Mantilla, D. Mason, P. McBride, P. Merkel, S. Mrenna, S. Nahn, V. O'Dell, V. Papadimitriou, K. Pedro, C. Pena[55], O. Prokofyev, F. Ravera, A. Reinsvold Hall, L. Ristori, B. Schneider, E. Sexton-Kennedy, N. Smith, A. Soha, L. Spiegel, S. Stoynev, J. Strait, L. Taylor, S. Tkaczyk, N.V. Tran, L. Uplegger, E.W. Vaandering, H.A. Weber

University of Florida, Gainesville, U.S.A.

D. Acosta, P. Avery, D. Bourilkov, L. Cadamuro, V. Cherepanov, F. Errico, R.D. Field, D. Guerrero, B.M. Joshi, M. Kim, J. Konigsberg, A. Korytov, K.H. Lo, K. Matchev, N. Menendez, G. Mitselmakher, D. Rosenzweig, K. Shi, J. Sturdy, J. Wang, E. Yigitbasi, X. Zuo

Florida State University, Tallahassee, U.S.A.

T. Adams, A. Askew, D. Diaz, R. Habibullah, S. Hagopian, V. Hagopian, K.F. Johnson, R. Khurana, T. Kolberg, G. Martinez, H. Prosper, C. Schiber, R. Yohay, J. Zhang

JHEP12(2021)106

Florida Institute of Technology, Melbourne, U.S.A.

M.M. Baarmand, S. Butalla, T. Elkafrawy[16], M. Hohlmann, R. Kumar Verma, D. Noonan, M. Rahmani, M. Saunders, F. Yumiceva

University of Illinois at Chicago (UIC), Chicago, U.S.A.

M.R. Adams, L. Apanasevich, H. Becerril Gonzalez, R. Cavanaugh, X. Chen, S. Dittmer, O. Evdokimov, C.E. Gerber, D.A. Hangal, D.J. Hofman, C. Mills, G. Oh, T. Roy, M.B. Tonjes, N. Varelas, J. Viinikainen, X. Wang, Z. Wu, Z. Ye

The University of Iowa, Iowa City, U.S.A.

M. Alhusseini, K. Dilsiz[88], S. Durgut, R.P. Gandrajula, M. Haytmyradov, V. Khristenko, O.K. Köseyan, J.-P. Merlo, A. Mestvirishvili[89], A. Moeller, J. Nachtman, H. Ogul[90], Y. Onel, F. Ozok[91], A. Penzo, C. Snyder, E. Tiras[92], J. Wetzel

Johns Hopkins University, Baltimore, U.S.A.

O. Amram, B. Blumenfeld, L. Corcodilos, M. Eminizer, A.V. Gritsan, S. Kyriacou, P. Maksimovic, J. Roskes, M. Swartz, T.Á. Vámi

The University of Kansas, Lawrence, U.S.A.

C. Baldenegro Barrera, P. Baringer, A. Bean, A. Bylinkin, T. Isidori, S. Khalil, J. King, G. Krintiras, A. Kropivnitskaya, C. Lindsey, N. Minafra, M. Murray, C. Rogan, C. Royon, S. Sanders, E. Schmitz, J.D. Tapia Takaki, Q. Wang, J. Williams, G. Wilson

Kansas State University, Manhattan, U.S.A.

S. Duric, A. Ivanov, K. Kaadze, D. Kim, Y. Maravin, T. Mitchell, A. Modak

Lawrence Livermore National Laboratory, Livermore, U.S.A.

F. Rebassoo, D. Wright

University of Maryland, College Park, U.S.A.

E. Adams, A. Baden, O. Baron, A. Belloni, S.C. Eno, Y. Feng, N.J. Hadley, S. Jabeen, R.G. Kellogg, T. Koeth, A.C. Mignerey, S. Nabili, M. Seidel, A. Skuja, S.C. Tonwar, L. Wang, K. Wong

Massachusetts Institute of Technology, Cambridge, U.S.A.

D. Abercrombie, R. Bi, S. Brandt, W. Busza, I.A. Cali, Y. Chen, M. D'Alfonso, G. Gomez Ceballos, M. Goncharov, P. Harris, M. Hu, M. Klute, D. Kovalskyi, J. Krupa, Y.-J. Lee, P.D. Luckey, B. Maier, A.C. Marini, C. Mironov, X. Niu, C. Paus, D. Rankin, C. Roland, G. Roland, Z. Shi, G.S.F. Stephans, K. Tatar, D. Velicanu, J. Wang, T.W. Wang, Z. Wang, B. Wyslouch

University of Minnesota, Minneapolis, U.S.A.

R.M. Chatterjee, A. Evans, P. Hansen, J. Hiltbrand, Sh. Jain, M. Krohn, Y. Kubota, Z. Lesko, J. Mans, M. Revering, R. Rusack, R. Saradhy, N. Schroeder, N. Strobbe, M.A. Wadud

University of Mississippi, Oxford, U.S.A.

J.G. Acosta, S. Oliveros

JHEP12(2021)106

University of Nebraska-Lincoln, Lincoln, U.S.A.

K. Bloom, M. Bryson, S. Chauhan, D.R. Claes, C. Fangmeier, L. Finco, F. Golf, J.R. González Fernández, C. Joo, I. Kravchenko, J.E. Siado, G.R. Snow[†], W. Tabb, F. Yan

State University of New York at Buffalo, Buffalo, U.S.A.

G. Agarwal, H. Bandyopadhyay, L. Hay, I. Iashvili, A. Kharchilava, C. McLean, D. Nguyen, J. Pekkanen, S. Rappoccio

Northeastern University, Boston, U.S.A.

G. Alverson, E. Barberis, C. Freer, Y. Haddad, A. Hortiangtham, J. Li, G. Madigan, B. Marzocchi, D.M. Morse, V. Nguyen, T. Orimoto, A. Parker, L. Skinnari, A. Tishelman-Charny, T. Wamorkar, B. Wang, A. Wisecarver, D. Wood

Northwestern University, Evanston, U.S.A.

S. Bhattacharya, J. Bueghly, Z. Chen, A. Gilbert, T. Gunter, K.A. Hahn, N. Odell, M.H. Schmitt, K. Sung, M. Velasco

University of Notre Dame, Notre Dame, U.S.A.

R. Bucci, N. Dev, R. Goldouzian, M. Hildreth, K. Hurtado Anampa, C. Jessop, K. Lannon, N. Loukas, N. Marinelli, I. Mcalister, F. Meng, K. Mohrman, Y. Musienko[48], R. Ruchti, P. Siddireddy, M. Wayne, A. Wightman, M. Wolf, L. Zygala

The Ohio State University, Columbus, U.S.A.

J. Alimena, B. Bylsma, B. Cardwell, L.S. Durkin, B. Francis, C. Hill, A. Lefeld, B.L. Winer, B.R. Yates

Princeton University, Princeton, U.S.A.

F.M. Addesa, B. Bonham, P. Das, G. Dezoort, P. Elmer, A. Frankenthal, B. Greenberg, N. Haubrich, S. Higginbotham, A. Kalogeropoulos, G. Kopp, S. Kwan, D. Lange, M.T. Lucchini, D. Marlow, K. Mei, I. Ojalvo, J. Olsen, C. Palmer, D. Stickland, C. Tully

University of Puerto Rico, Mayaguez, U.S.A.

S. Malik, S. Norberg

Purdue University, West Lafayette, U.S.A.

A.S. Bakshi, V.E. Barnes, R. Chawla, S. Das, L. Gutay, M. Jones, A.W. Jung, S. Karmarkar, M. Liu, G. Negro, N. Neumeister, C.C. Peng, S. Piperov, A. Purohit, J.F. Schulte, M. Stojanovic[17], J. Thieman, F. Wang, R. Xiao, W. Xie

Purdue University Northwest, Hammond, U.S.A.

J. Dolen, N. Parashar

Rice University, Houston, U.S.A.

A. Baty, S. Dildick, K.M. Ecklund, S. Freed, F.J.M. Geurts, A. Kumar, W. Li, B.P. Padley, R. Redjimi, J. Roberts[†], W. Shi, A.G. Stahl Leiton

University of Rochester, Rochester, U.S.A.

A. Bodek, P. de Barbaro, R. Demina, J.L. Dulemba, C. Fallon, T. Ferbel, M. Galanti, A. Garcia-Bellido, O. Hindrichs, A. Khukhunaishvili, E. Ranken, R. Taus

JHEP12(2021)106

Rutgers, The State University of New Jersey, Piscataway, U.S.A.

B. Chiarito, J.P. Chou, A. Gandrakota, Y. Gershtein, E. Halkiadakis, A. Hart, M. Heindl, E. Hughes, S. Kaplan, O. Karacheban[24], I. Laflotte, A. Lath, R. Montalvo, K. Nash, M. Osherson, S. Salur, S. Schnetzer, S. Somalwar, R. Stone, S.A. Thayil, S. Thomas, H. Wang

University of Tennessee, Knoxville, U.S.A.

H. Acharya, A.G. Delannoy, S. Spanier

Texas A&M University, College Station, U.S.A.

O. Bouhali[93], M. Dalchenko, A. Delgado, R. Eusebi, J. Gilmore, T. Huang, T. Kamon[94], H. Kim, S. Luo, S. Malhotra, R. Mueller, D. Overton, D. Rathjens, A. Safonov

Texas Tech University, Lubbock, U.S.A.

N. Akchurin, J. Damgov, V. Hegde, S. Kunori, K. Lamichhane, S.W. Lee, T. Mengke, S. Muthumuni, T. Peltola, S. Undleeb, I. Volobouev, Z. Wang, A. Whitbeck

Vanderbilt University, Nashville, U.S.A.

E. Appelt, S. Greene, A. Gurrola, W. Johns, C. Maguire, A. Melo, H. Ni, K. Padeken, F. Romeo, P. Sheldon, S. Tuo, J. Velkovska

University of Virginia, Charlottesville, U.S.A.

M.W. Arenton, B. Cox, G. Cummings, J. Hakala, R. Hirosky, M. Joyce, A. Ledovskoy, A. Li, C. Neu, B. Tannenwald, E. Wolfe

Wayne State University, Detroit, U.S.A.

P.E. Karchin, N. Poudyal, P. Thapa

University of Wisconsin — Madison, Madison, WI, U.S.A.

K. Black, T. Bose, J. Buchanan, C. Caillol, S. Dasu, I. De Bruyn, P. Everaerts, C. Galloni, H. He, M. Herndon, A. Hervé, U. Hussain, A. Lanaro, A. Loeliger, R. Loveless, J. Madhusudanan Sreekala, A. Mallampalli, A. Mohammadi, D. Pinna, A. Savin, V. Shang, V. Sharma, W.H. Smith, D. Teague, S. Trembath-Reichert, W. Vetens

†: Deceased
1: Also at TU Wien, Wien, Austria
2: Also at Institute of Basic and Applied Sciences, Faculty of Engineering, Arab Academy for Science, Technology and Maritime Transport, Alexandria, Egypt, Alexandria, Egypt
3: Also at Université Libre de Bruxelles, Bruxelles, Belgium
4: Also at IRFU, CEA, Université Paris-Saclay, Gif-sur-Yvette, France
5: Also at Universidade Estadual de Campinas, Campinas, Brazil
6: Also at Federal University of Rio Grande do Sul, Porto Alegre, Brazil
7: Also at UFMS, Nova Andradina, Brazil
8: Also at Nanjing Normal University Department of Physics, Nanjing, China
9: Now at The University of Iowa, Iowa City, U.S.A.
10: Also at University of Chinese Academy of Sciences, Beijing, China
11: Also at Institute for Theoretical and Experimental Physics named by A.I. Alikhanov of NRC 'Kurchatov Institute', Moscow, Russia

JHEP12(2021)106

12: Also at Joint Institute for Nuclear Research, Dubna, Russia
13: Also at Cairo University, Cairo, Egypt
14: Also at Suez University, Suez, Egypt
15: Now at British University in Egypt, Cairo, Egypt
16: Now at Ain Shams University, Cairo, Egypt
17: Also at Purdue University, West Lafayette, U.S.A.
18: Also at Université de Haute Alsace, Mulhouse, France
19: Also at Erzincan Binali Yildirim University, Erzincan, Turkey
20: Also at CERN, European Organization for Nuclear Research, Geneva, Switzerland
21: Also at RWTH Aachen University, III. Physikalisches Institut A, Aachen, Germany
22: Also at University of Hamburg, Hamburg, Germany
23: Also at Department of Physics, Isfahan University of Technology, Isfahan, Iran, Isfahan, Iran
24: Also at Brandenburg University of Technology, Cottbus, Germany
25: Also at Skobeltsyn Institute of Nuclear Physics, Lomonosov Moscow State University, Moscow, Russia
26: Also at Physics Department, Faculty of Science, Assiut University, Assiut, Egypt
27: Also at Eszterhazy Karoly University, Karoly Robert Campus, Gyongyos, Hungary
28: Also at Institute of Physics, University of Debrecen, Debrecen, Hungary
29: Also at Institute of Nuclear Research ATOMKI, Debrecen, Hungary
30: Also at MTA-ELTE Lendület CMS Particle and Nuclear Physics Group, Eötvös Loránd University, Budapest, Hungary
31: Also at Wigner Research Centre for Physics, Budapest, Hungary
32: Also at IIT Bhubaneswar, Bhubaneswar, India
33: Also at Institute of Physics, Bhubaneswar, India
34: Also at G.H.G. Khalsa College, Punjab, India
35: Also at Shoolini University, Solan, India
36: Also at University of Hyderabad, Hyderabad, India
37: Also at University of Visva-Bharati, Santiniketan, India
38: Also at Indian Institute of Technology (IIT), Mumbai, India
39: Also at Deutsches Elektronen-Synchrotron, Hamburg, Germany
40: Also at Sharif University of Technology, Tehran, Iran
41: Also at Department of Physics, University of Science and Technology of Mazandaran, Behshahr, Iran
42: Now at INFN Sezione di Bari, Università di Bari, Politecnico di Bari, Bari, Italy
43: Also at Italian National Agency for New Technologies, Energy and Sustainable Economic Development, Bologna, Italy
44: Also at Centro Siciliano di Fisica Nucleare e di Struttura Della Materia, Catania, Italy
45: Also at Università di Napoli 'Federico II', Napoli, Italy
46: Also at Riga Technical University, Riga, Latvia
47: Also at Consejo Nacional de Ciencia y Tecnología, Mexico City, Mexico
48: Also at Institute for Nuclear Research, Moscow, Russia
49: Now at National Research Nuclear University 'Moscow Engineering Physics Institute' (MEPhI), Moscow, Russia
50: Also at St. Petersburg State Polytechnical University, St. Petersburg, Russia
51: Also at University of Florida, Gainesville, U.S.A.
52: Also at Imperial College, London, United Kingdom
53: Also at P.N. Lebedev Physical Institute, Moscow, Russia
54: Also at Moscow Institute of Physics and Technology, Moscow, Russia

JHEP12(2021)106

55: Also at California Institute of Technology, Pasadena, U.S.A.
56: Also at Budker Institute of Nuclear Physics, Novosibirsk, Russia
57: Also at Faculty of Physics, University of Belgrade, Belgrade, Serbia
58: Also at Trincomalee Campus, Eastern University, Sri Lanka, Nilaveli, Sri Lanka
59: Also at INFN Sezione di Pavia, Università di Pavia, Pavia, Italy, Pavia, Italy
60: Also at National and Kapodistrian University of Athens, Athens, Greece
61: Also at Universität Zürich, Zurich, Switzerland
62: Also at Ecole Polytechnique Fédérale Lausanne, Lausanne, Switzerland
63: Also at Stefan Meyer Institute for Subatomic Physics, Vienna, Austria
64: Also at Laboratoire d'Annecy-le-Vieux de Physique des Particules, IN2P3-CNRS, Annecy-le-Vieux, France
65: Also at Şırnak University, Sirnak, Turkey
66: Also at Department of Physics, Tsinghua University, Beijing, China
67: Also at Near East University, Research Center of Experimental Health Science, Nicosia, Turkey
68: Also at Beykent University, Istanbul, Turkey
69: Also at Istanbul Aydin University, Application and Research Center for Advanced Studies (App. & Res. Cent. for Advanced Studies), Istanbul, Turkey
70: Also at Mersin University, Mersin, Turkey
71: Also at Piri Reis University, Istanbul, Turkey
72: Also at Adiyaman University, Adiyaman, Turkey
73: Also at Ozyegin University, Istanbul, Turkey
74: Also at Izmir Institute of Technology, Izmir, Turkey
75: Also at Necmettin Erbakan University, Konya, Turkey
76: Also at Bozok Universitetesi Rektörlügü, Yozgat, Turkey
77: Also at Marmara University, Istanbul, Turkey
78: Also at Milli Savunma University, Istanbul, Turkey
79: Also at Kafkas University, Kars, Turkey
80: Also at Istanbul Bilgi University, Istanbul, Turkey
81: Also at Hacettepe University, Ankara, Turkey
82: Also at Vrije Universiteit Brussel, Brussel, Belgium
83: Also at School of Physics and Astronomy, University of Southampton, Southampton, United Kingdom
84: Also at IPPP Durham University, Durham, United Kingdom
85: Also at Monash University, Faculty of Science, Clayton, Australia
86: Also at Bethel University, St. Paul, Minneapolis, U.S.A., St. Paul, U.S.A.
87: Also at Karamanoğlu Mehmetbey University, Karaman, Turkey
88: Also at Bingol University, Bingol, Turkey
89: Also at Georgian Technical University, Tbilisi, Georgia
90: Also at Sinop University, Sinop, Turkey
91: Also at Mimar Sinan University, Istanbul, Istanbul, Turkey
92: Also at Erciyes University, Kayseri, Turkey
93: Also at Texas A&M University at Qatar, Doha, Qatar
94: Also at Kyungpook National University, Daegu, Korea

JHEP12(2021)106